MODE-MODE INTERFERENCE IN OPTICAL FIBERS: ANALYSIS AND EXPERIMENT

by

N.K.Shankaranarayanan

Thesis submitted to the Faculty of the

Virginia Polytechnic Institute and State University

in partial fulfillment of the requirements for the degree of

Master of Science

in

Electrical Engineering

APPROVED:

R.O.Claus, Chairman

T.C.Poon

A.Safaai-Jazi

March 12, 1987

Blacksburg, Virginia

MODE-MODE INTERFERENCE IN OPTICAL FIBERS: ANALYSIS AND EXPERIMENT

by

N.K.Shankaranarayanan

R.O.Claus, Chairman

Electrical Engineering

(ABSTRACT)

Interference between the modes of an optical fiber generates specific mode (intensity) patterns which get modulated by disturbances in the optical fiber system. Mode-mode interference has been analyzed from first principles and a model based on differential phase modulation presented. Mode-mode interference effects such as intensity modulation of the mode patterns are directly related to differential phase modulation between modes which arises due to the difference between the propagation constants of the constituent modes. Practical implementation of modal methods involves selective launching of modes and processing of the output pattern to demodulate the information.

Axial strain has been chosen as the modulating mechanism in experiments designed to quantify mode-mode interference effects. Quasi-statically varying strain as well as vibrational strain was used to study 'dc' and 'ac' mechanisms. Specific mode combinations have been excited and their radiation patterns identified. Mode pattern changes have been described. Experimental observations and results correlate very well with analysis.

Acknowledgements

I thank my advisor and friend Dr. Richard O. Claus very deeply for the invaluable guidance, encouragement and motivation he gave me.

I wish to thank Dr. Ahmad Safaai-Jazi for his guidance and help in understanding subtle concepts of modal analysis. I thank Dr. T.C.Poon for being on my advisory committee.

I also wish to specially thank for doing the figures and , and for helping me at various points of my work in this fascinating subject.

This work has been sponsored in part by the Center for Innovative Technology.

Table of Contents

List of Illustrations

1.0 Introduction

The optical fiber was developed as a means of propagating light through a waveguide primarily for information transmission. This lightwave medium is a fascinating marriage of waveguide and optical sciences.

Of basic interest in fiber optics technology is the analysis of the propagation mechanisms of light in an optical waveguide. The fiber is modelled as a cylindrical circular dielectric waveguide for electromagnetic analysis. The principle of guidance is total internal reflection at the interface of the core and the cladding, the concentric regions of the fiber which have slightly differing refractive indices. The field distributions, propagation mechanisms, intensity and polarization of light guided in such fibers are major considerations in this analysis.

1.1 Optical Fiber Sensing

Optical fiber communications technology uses the fiber as a low-loss, wideband medium for information transmission and seeks minimization of the fiber response to external perturbations and

factors. On the contrary, *optical fiber sensing* is based on these very effects of external factors on lightwave propagation.

Fiber optic sensors exploit the effects of perturbations and external factors on the light in the fiber. Specifically, the intensity, phase and polarization are available for alteration and the detection of these changes is the basis for fiber optic sensors. Phase modulated sensors are unparalleled in sensitivity. Conventional phase modulation schemes employ various mechanisms to modulate the phase of the lightwave using the parameter to be measured. Comparing the varying phase to a reference phase i.e. demodulating the phase information generates a sensor output signal. This is illustrated in the classic Mach-Zehnder interferometer in Figure 1 on page 52. In this scheme, a single source feeds light into two different single-mode fibers, i.e. the sensing arm and the reference arm of the interferometer. A change in phase in the sensing arm can be demodulated and related to the external cause of the phase change. At optical frequencies, this demodulation is achieved by measuring the intensity of the interference field and detecting changes. In the Mach-Zehnder interferometer, the field magnitudes change in time and space because of the phase change and thus cause a change in the interference pattern.

1.2 Modal Domain Sensing

It is well established that there exist in the waveguide various modes of electromagnetic wave propagation not unlike the modes of metal waveguides. Modal analysis is a standard technique in waveguide theory. Mode effects like modal noise and intermodal dispersion lead to a decrease in communications system performance.

The modal field structure can be used to extract information regarding any change in the fiber characteristics. We define **modal domain sensing** as any sensing technique that is based on the in-

terference between modes or mode combinations. The modulation of the phase of one mode with respect to that of another as a reference is used as a sensor signal. One way of implementing this method is to use some unique combination of modes that display modulation characteristics suitable for sensing. Information could then be extracted from this (differential) mode-mode interference phenomenon.

Practical problems like fading and phase fluctuations in the reference arm plague dual-beam interferometry. These problems are due to the different environments around the two optical fibers. Single-beam interferometers using some kind of "self-referencing" can eliminate these common-mode problems. Modal domain sensors are, by definition, such single fiber sensors and they could be used as "self-referenced interferometers."

This report examines the theoretical and experimental aspects of mode-mode interference and mode modulation. Chapters 2 and 3 describe optical waveguide and mode theory. Only relevant matter is described and results easily available in the literature are quoted without proof. Chapter 3 also describes some specific mode combinations important to the experiments described later. Chapter 4 reviews mode-mode interference concepts and proposes a mathematical model for some experimentally observed effects. Chapters 5 and 6 report the experiments performed as well as the results and discussion. Chapter 7 concludes the report. Figures are included and references cited at the end of the report.

2.0 Optical Waveguide Theory

A typical optical fiber is shown in Figure 2 on page 53. The fiber has a circular cross-section and is typically made of glass (fused silica). There is a central core surrounded by a cladding. The refractive index of the core is slightly higher than that of the cladding. The fiber is covered by a protective polymer coating. Typical dimensions for the core/cladding/jacket diameters are 9/125/250 μ and 50/125/250 μ for single-mode and multi-mode optical fibers respectively. As the names suggest, a single-mode optical fiber supports only one mode while a multi-mode fiber supports numerous modes. Modes are explained in detail in Chapter 3.

The refractive index profile (RIP) for the core and cladding regions is also used to characterize an optical fiber. We shall deal only with the step-index type. Based on the refractive indices of the core and cladding (n_1 and n_2), the wavelength of operation (λ) and the core radius (a), we can define the V-parameter for an optical fiber as

$$V = \frac{2\pi}{\lambda}\sqrt{n_1^2 - n_2^2}\,.$$

The range of single-mode operation is $V < 2.405$ and that of multi-mode is typically $V > > 5$ We term the intermediate $2.405 < V < 5$ range as that of few-mode operation. Most of the matter

discussed in this report addresses few-mode optical fibers. In this chapter, we shall model the optical fiber as a waveguide and set up the waveguide electromagnetic equations.

An optical fiber can be treated as a circular dielectric cylindrical waveguide for the purpose of electromagnetic analysis. It is best to formulate the general wave equations and then apply them to dielectrics and circular dielectric waveguides. This approach is similar to the ones employed in microwave waveguide analysis.

2.1 Waveguide Equations for Dielectric Cylinders

We reproduce here the differential form of Maxwell's equations for instantaneous field quantities.

$$\begin{aligned} \nabla \times \mathbf{E}(t) &= -\frac{\partial \mathbf{B}(t)}{\partial t} \\ \nabla \times \mathbf{H}(t) &= \frac{\partial \mathbf{D}(t)}{\partial t} + \mathbf{J}(t) \\ \nabla \cdot \mathbf{B} &= 0 \\ \nabla \cdot \mathbf{D} &= \rho_v \end{aligned} \tag{2.1.1}$$

Henceforth, this analysis uses the complex phasor notation where the instantaneous field quantities are related to the complex phasors by the relation

$$\mathbf{E}(t) = \text{Re}\,[\mathbf{E}\exp(j\omega t)]. \tag{2.1.2}$$

This relation is equivalent to three scalar equations for the three spatial components of the vectors. We shall be dealing with linear, isotropic, homogeneous and source-free perfect dielectrics to obtain ideal solutions. In general, graded-index optical fibers are not homogeneous and special mathematical techniques are required to obtain solutions in such cases. We shall be considering step-index optical fibers. This is not very restrictive since this work relates directly to few-mode fibers

which are typically step-index. The field quantities can be considered to be time-harmonic without loss of generality. For such a case, we can write the Maxwell's equations in complex notation as under:

$$\begin{aligned} \nabla \mathbf{x}\, \mathbf{E} &= -j\mu\omega\mathbf{H} \\ \nabla \mathbf{x}\, \mathbf{H} &= j\omega\varepsilon\mathbf{E} \\ \nabla \cdot \mathbf{B} &= 0 \\ \nabla \cdot \mathbf{D} &= 0 \end{aligned} \tag{2.1.3}$$

where μ, the permeability, and ε , the permittivity, are constants.

For optical materials, we also have the index of refraction n given by

$$n = \sqrt{\varepsilon_r} = \sqrt{\varepsilon/\varepsilon_0}\,. \tag{2.1.4}$$

Since we are analyzing cylindrical waveguides, it is convenient to use cylindrical coordinates as shown in Figure 3 on page 54. We expect to deal with wave propagation down the cylindrical waveguide. So we align our z-axis along the axis of the cylinder and seek solutions for wave propagation along the z-axis.

From (2.1.3), we have the well-known Helmholtz equation describing electromagnetic wave phenomena.

$$\begin{aligned} \nabla^2\mathbf{E} + k^2\mathbf{E} &= 0 \\ k^2 &= \omega^2\mu\varepsilon = 2\pi/\lambda^2. \end{aligned} \tag{2.1.5}$$

A general solution to the wave equation is given by

$$\begin{aligned} \mathbf{E}(\mathbf{r},t) &= E_0(\mathbf{r})\exp[j(\omega t - \mathbf{k}\cdot\mathbf{r})]\,\mathbf{u}_e \\ \mathbf{k} &= k\mathbf{u}_k \\ \mathbf{r} &= x\mathbf{u}_x + y\mathbf{u}_y + z\mathbf{u}_z = \rho\mathbf{u}_\rho + \varphi\mathbf{u}_\varphi + z\mathbf{u}_z \\ \mathbf{u}_k &= \text{unit vector in the direction of propagation} \\ \mathbf{u}_e &= \text{unit vector in the direction of the E field} \end{aligned} \tag{2.1.6}$$

In general, we expect to have field solutions which are functions of ρ, φ and z. There should be a 2π periodicity in φ since it is the azimuthal angle. We also expect fields to propagate in the $+z$ direction. It is worthwhile to investigate this on a mathematical basis.

All cartesian components of the field satisfy (2.1.5). For any cartesian scalar component (or the cylindrical z-component) ψ , we can expand ∇^2 as [1]

$$\frac{1}{\rho}\frac{\partial}{\partial\rho}\left(\rho\frac{\partial\psi}{\partial\rho}\right) + \frac{1}{\rho^2}\frac{\partial^2\psi}{\partial\varphi^2} + \frac{\partial^2\psi}{\partial z^2} + k^2\psi = 0. \tag{2.1.7}$$

Separating the variables,

$$\psi = \psi_0 R(\rho)\Phi(\varphi)Z(z). \tag{2.1.8}$$

From (2.1.7) and (2.1.8), we get [1]

$$\frac{1}{\rho R}\frac{\partial}{\partial\rho}\left(\rho\frac{dR}{d\rho}\right) + \frac{1}{\rho^2\Phi}\frac{d^2\varphi}{d\varphi^2} + \frac{1}{Z}\frac{d^2Z}{dz^2} + k^2 = 0. \tag{2.1.9}$$

Note that this equation is valid for all ρ, φ and z. The third term in (2.1.9) is independent of ρ and φ. Using that to write it as a constant and multiplying the equation by ρ^2, we have the second term independent of ρ and z, and so we can write

$$\begin{aligned} \frac{d^2Z}{dz^2} &= -h^2Z \\ \frac{d^2\Phi}{d\varphi^2} &= -\nu^2\Phi \\ h &= \text{some constant} > 0 \\ \nu &= \text{some constant.} \end{aligned} \tag{2.1.10}$$

Since we are seeking solutions of waves propagating along the $+z$-axis, we write using convention,

$$\begin{aligned} Z &= e^{-jhz}, \text{ and} \\ \Phi &= e^{j\nu\varphi}. \end{aligned} \tag{2.1.11}$$

Defining

$$\kappa^2 = k^2 - h^2 \tag{2.1.12}$$

we have from (2.1.9) and (2.1.10)

$$\rho\frac{\partial}{\partial\rho}\left(\rho\frac{dR}{d\rho}\right) + \left[(\kappa\rho)^2 - \nu^2\right]R = 0 \tag{2.1.13}$$

Possible solutions to the above Bessel's equation of order ν are Bessel functions. Thus we write

$$\begin{aligned} R &= Z_\nu(\kappa\rho), \text{ and} \\ \psi &= \psi_{\nu,h}\, Z_\nu(\kappa\rho)e^{j\nu\varphi}e^{-jhz}. \end{aligned} \tag{2.1.14}$$

Since we expected propagation in the $+z$ direction, we compare (2.1.14) with (2.1.6) to get

$$\begin{aligned} h &= \mathbf{k}\cdot\mathbf{u}_z \\ &= \text{longitudinal propagation constant.} \end{aligned} \tag{2.1.15}$$

From (2.1.12) and Figure 4 on page 55, we have κ as the transverse propagational constant.

Since we must have 2π azimuthal symmetry ν must be an integer. Accordingly, we change notation to n to reflect this fact. So the axial field component (z-component) can be written as

$$F_n = \psi_n = C_n Z_n(\kappa\rho)e^{jn\varphi - jhz + j\omega t}. \tag{2.1.16}$$

We have determined the nature of the field solutions to the waveguide equations. In following sections, we apply these to step-index optical fibers.

2.2 *Circularly Polarized Field Components*

In this section, we develop an alternative representation of the transverse field based on the formalism in Ref [2]. In the practical world, only the intensity and polarization of the field at the fiber endface can be observed either as near-field or far-field patterns. Both of these depend on the transverse components of the field.

We have, in general, elliptical polarization of the transverse field and can represent it as a combination of circularly polarized components. This makes for better physical interpretation than determining the x,y,z or ρ, φ,z components.

We define [2]

$$\mathbf{E}_{\pm} = E_{\pm}(\mathbf{u}_x \mp j\mathbf{u}_y)e^{j(\omega t - hz).} \tag{2.2.1}$$

For E_+, we have left-handed circular polarization (LHCP) and for E_-, we have right-handed circular polarization (RHCP) [1]. Similarly,

$$\mathbf{H}_{\pm} = H_{\pm}(\mathbf{u}_x \mp j\mathbf{u}_y)e^{j(\omega t - hz)} \tag{2.2.2}$$

The real fields of **E** are

$$\begin{aligned} \text{Re}\,[\mathbf{E}_{\pm}] &= |E_{\pm}|\left[\mathbf{u}_x\cos(\omega t - hz + \delta_{\pm}) + \mathbf{u}_y\sin(\omega t - hz + \delta_{\pm})\right] \\ \text{where } E_{\pm} &= |E_{\pm}|e^{j\delta_{\pm}}. \end{aligned} \tag{2.2.3}$$

Note that the RHCP and LHCP components are orthogonal in the power sense because

$$\mathbf{E}_{\pm} \times \mathbf{H}_{\mp} = 0. \tag{2.2.4}$$

We define for easier writing

$$\mathbf{v}_{\pm} = \mathbf{u}_x \mp j\mathbf{u}_y. \tag{2.2.5}$$

We must keep in mind that these are not unit vectors. Now, we write

$$\begin{aligned} \mathbf{E} &= \mathbf{E}_\rho + \mathbf{E}_\varphi + \mathbf{E}_z \\ &= \mathbf{E}_+ + \mathbf{E}_- + \mathbf{E}_z \\ &= E_+\mathbf{v}_+ + E_-\mathbf{v}_- + E_z\mathbf{u}_z. \end{aligned} \tag{2.2.6}$$

We thus get the following relations

$$\begin{aligned} E_{\pm} &= \frac{E_x \pm jE_y}{2} \\ E_{\pm}e^{\mp j\varphi} &= \frac{E_\rho \pm jE_\varphi}{2} \\ E_x &= E_+ + E_- \\ jE_y &= E_+ - E_-. \end{aligned} \tag{2.2.7}$$

From this representation, we can easily determine the state of polarization. Comparing $|E|_+$ and $|E_-|$, we know if the field is LHP or RHP. The magnitudes also indicate the ellipticity of the polarization ellipse and the phases δ_+ and δ_- indicate the orientation. Since polarization plays an important part in filtering information from observation of the fiber output patterns, this representation will be helpful later.

2.3 *Field Solutions in Step-index Optical Fibers*

The generalized field solutions obtained in section 2.1 can be used in Maxwell's equations with specific boundary conditions to analyze the step-index optical fiber.

We can translate the vector operator ∇ as [2]

$$
\begin{aligned}
\nabla &= \mathbf{u}_x \frac{\partial}{\partial x} + \mathbf{u}_y \frac{\partial}{\partial y} + \mathbf{u}_z \frac{\partial}{\partial z} \\
\nabla &= \mathbf{u}_x \nabla_x + \mathbf{u}_y \nabla_y + \mathbf{u}_z \nabla_z \\
&= \mathbf{v}_+ \nabla_+ + \mathbf{v}_- \nabla_- + \mathbf{u}_z \nabla_z \\
\text{where } \nabla_\pm &= \frac{1}{2} \mathbf{v}_\pm^* \cdot \nabla \\
&= \frac{1}{2} e^{j\varphi} \left[\frac{\partial}{\partial \rho} + \frac{j}{\rho} \frac{\partial}{\partial \varphi} \right] \\
&= \frac{1}{2} \left[\frac{\partial}{\partial x} + \frac{\partial}{\partial y} \right].
\end{aligned}
\tag{2.3.1}
$$

Since we have from (2.1.16) that the axial field component is of the form

$$
F_n = \psi_n = C_n Z_n(\kappa\rho) e^{jn\varphi - jhz + j\omega t}, \tag{2.3.2}
$$

let us take

$$
\begin{aligned}
E_z &= AF_n \text{ and} \\
H_z &= BF_n.
\end{aligned}
\tag{2.3.3}
$$

If we write Maxwell's equations (2.1.3) in terms of the circularly polarized components using (2.3.1) and substitute (2.3.3), we get the following relations [2].

$$
\begin{aligned}
E_z &= AF_n \\
H_z &= BF_n \\
E_+ &= \left(\frac{1}{2\kappa}\right)(jhA + \omega\mu B)F_{n+1} \\
H_+ &= -\left(\frac{1}{2\kappa}\right)(\omega\varepsilon A - jhB)F_{n+1} \\
E_- &= -\left(\frac{1}{2\kappa}\right)(jhA - \omega\mu B)F_{n-1} \\
H_- &= -\left(\frac{1}{2\kappa}\right)(\omega\varepsilon A + jhB)F_{n-1}.
\end{aligned}
\tag{2.3.4}
$$

To simplify the above, we multiply by $\frac{2\kappa}{jh}$ and set

$$\alpha = \frac{\omega\mu B}{jhA}. \tag{2.3.5}$$

Then we have [2]

$$\begin{aligned} E_{\pm} &= \pm (1 \pm \alpha) A F_{n\pm 1} \\ H_{\pm} &= \left(\frac{jh}{\omega\mu}\right)\left[\left(\frac{k^2}{h^2}\right) \pm \alpha\right] A F_{n\pm 1} \\ E_z &= \left(\frac{2\kappa}{jh}\right) A F_n \\ H_z &= \left(\frac{jh}{\omega\mu}\right)\alpha E_z \\ F_n &= Z_n(\kappa\rho) e^{jn\varphi + j\omega t - jhz}. \end{aligned} \tag{2.3.6}$$

These can be used to describe fields in both the core and cladding. Of course, they can be finally accepted only if the conditions at the boundary can be satisfied. Using the suffix 1 for the core and 2 for the cladding, we first note the following.

$$\begin{aligned} \varepsilon_1 &\neq \varepsilon_2 \\ \mu_1 &= \mu_2 = \mu \\ k_1 &\neq k_2. \end{aligned}$$

The solutions describe time-harmonic fields propagating along $+z$ axis. Imposing phase synchronism at the interface

$$h_1 = k_1 \cos\theta_1 = k_2 \cos\theta_2 = h_2 = h, \tag{2.3.7}$$

where θ_1 and θ_2 are the angles of the equivalent light ray with the interface in the core and the cladding. We thus have

$$h = k_1 \cos\theta_1 \leq k_1.$$

Also,

$$k_2 = k_1 \cos\theta_1 \qquad \theta_1 \geq \theta_c, \text{ and}$$
$$k_2 = k_1 \cos\theta_c \leq k_1 \cos\theta_1 \leq h \qquad \theta_1 \leq \theta_c$$

Thus, for total internal reflection at the core-claddding interface ($\theta_1 \leq \theta_c$),

$$\begin{aligned} & k_2 \leq h \leq k_1 \\ & \kappa_1^2 \geq 0 \\ & \kappa_2^2 \leq 0 \\ & \kappa_{1,2} = \pm \left(k_{1,2}^2 - h^2\right)^{\frac{1}{2}}. \end{aligned} \tag{2.3.8}$$

For the sign of the radical above, we will use the convention that Re [κ] > 0 [1]. In the case that κ becomes imaginary, we introduce a little loss in k and take

$$k = \lim_{k'' \to 0} k' - jk''$$

to apply this convention. Thus, for imaginary κ_2, $\kappa_2 = -jq$ where $q = \sqrt{k_2^2 - h^2}$ is real. In general,

$$A_1 \neq A_2 \text{ and}$$
$$|\kappa_1| \neq |\kappa_2|$$

Now, we can apply the boundary conditions of the step-index optical fiber to our solutions.

1. The fields must be finite in the core at $\rho = 0$. This limits our choice of the Bessel function and thus we have

$$\begin{aligned} & Z_n(\kappa_1\rho) = J_n(\kappa_1\rho), \text{ where} \\ & J_n = \text{Bessel function of the first kind .} \end{aligned} \tag{2.3.8}$$

2. The fields in the cladding that we are interested in are evanescent fields. Because the guiding mechanism is total internal reflection, the field should satisfy radiation conditions and decay

exponentially far away from the core. Such behaviour can be described by the $H_n^{(2)}$, the Hankel function of the second kind. Note that if we had a different convention for imaginary κ i.e. $\kappa = jq$, then we would use $H_n^{(1)}$ the Hankel function of the first kind as in [3]. As in [6], we could also use K_n, the modified Bessel function of the second kind which is related to $H_n^{(2)}$ by

$$H_n^{(2)}(-jq) = (-j)^{-n-1}\left(\frac{2}{\pi}\right)K_n(q).$$

We thus have for the cladding

$$Z_n(\kappa_2\rho) = H_n^{(2)}(\kappa_2\rho) = H_n(\kappa_2\rho). \tag{2.3.9}$$

3. The tangential components of the fields in φ and z must be continuous at $\rho = a$. Using (2.3.6) and (2.3.7), we equate the z component to get [2]

$$\begin{aligned} A_2 &= \frac{A_1 u J_n(u)}{v H_n(v)}, \\ \text{where } u &= \kappa_1 a, \text{ and} \\ v &= \kappa_2 a. \end{aligned} \tag{2.3.10}$$

Using (2.2.7), (2.3.10), (2.3.6) and (2.3.7) and equating the φ components, we get [2]

$$\begin{gathered} (1+\alpha)(J_+ - H_+) = -(1-\alpha)(J_- - H_-) \\ \left(\frac{k_1^2}{h^2}\right)(J_+ - J_-) + \alpha(J_+ + J_-) = \left(\frac{k_2^2}{h^2}\right)(H_+ - H_-) + \alpha(H_+ - H_-), \\ \text{where } J_\pm = \frac{J_{n\pm1}(u)}{uJ_n(u)} \\ H_\pm = \frac{H_{n\pm1}(v)}{vH_n(v)}. \end{gathered} \tag{2.3.11}$$

We also have

$$u^2 - v^2 = \left(\frac{2\pi a}{\lambda}\right)^2(n_1^2 - n_2^2) = V^2. \tag{2.3.12}$$

Equations (2.3.11) gives us a characteristic equation which we can solve to determine the eigenvalues u and v of this boundary value problem. These are related to actual fiber characteristics by (2.3.12). The solutions can be used in our generalized field solutions that we summarize below. In the core, are

$$
\begin{aligned}
E_{\pm} &= \pm (1 \pm \alpha) A J_{n\pm 1}(\kappa_1 \rho) e^{j(n\pm 1)\varphi + j\omega t - jhz} \\
H_{\pm} &= \left(\frac{jh}{\omega\mu}\right)\left[\frac{\left(\frac{k_1^2}{h^2}\right) \pm \alpha}{1 \pm \alpha}\right] E_{\pm} \\
E_z &= \left(\frac{2\kappa_1}{jh}\right) A J_n(\kappa_1 \rho) e^{jn\varphi + j\omega t - jhz} \\
H_z &= \left(\frac{jh}{\omega\mu}\right)\alpha E_z \\
u &= \kappa_1 a \\
v &= \kappa_2 a \\
\kappa_1^2 &= k_1^2 - h^2 \\
\alpha &= \frac{\omega\mu B}{jhA}.
\end{aligned}
\tag{2.3.13}
$$

For the cladding we can use the above with the following transformations

$$
\begin{aligned}
J_p(\kappa_1 \rho) &\rightarrow H_p(\kappa_2 \rho),\ p = n-1, n, n+1 \\
\kappa_1 &\rightarrow \kappa_2 \\
u &\rightarrow v \\
k_1 &\rightarrow k_2 \\
\frac{A u J_n(u)}{v H_n(v)} &\rightarrow A.
\end{aligned}
\tag{2.3.14}
$$

For the evanescent fields arising from total internal reflection, we have $v = -jq$ where q is real . For this we can write [1]

$$
H_n(-jq) \cong j^{n+1} \frac{\sqrt{2}}{\sqrt{\pi q}} e^{-q} \text{ , for large q.} \tag{2.3.15}
$$

To analyze the intensity distribution of the mode fields at the fiber endface, we neglect end reflections and assume the fields to be the same as if the fiber were an infinite cylinder. This is valid for dielectric cylinders [2]. The intensity distribution is thus the time average of the z-component of the Poynting vector. Thus,

$$\begin{aligned} S_z &= \frac{\mathrm{Re}\,[\mathbf{E} \times \mathbf{H}^*] \cdot \mathbf{u}_z}{2} \\ &= \mathrm{Re}\,\left[(E_+ \mathbf{v}_+ + E_- \mathbf{v}_-) \times (H_+^* \mathbf{v}_+^* + H_-^* \mathbf{v}_-^*)\right]/2 \\ &= \mathrm{Im}\,[E_+ H_+^* - E_- H_-^*]. \end{aligned} \tag{2.3.16}$$

For $\rho < a$ we substitute (2.3.13) and get

$$\begin{aligned} S_z = \left(\frac{hAA^*}{\omega\mu}\right) &\left\{(1+\alpha)\left[\left(\frac{k_1^2}{h^2}\right) + \alpha\right] J_{n+1}^2(\kappa_1\rho)\right\} \\ &+ (1-\alpha)\left[\left(\frac{k_1^2}{h^2}\right) - \alpha\right] J_{n-1}^2(\kappa_1\rho). \end{aligned} \tag{2.3.17}$$

Having determined the nature of the field solutions, we will try to solve the characteristic equation to get unique solutions in the following sections.

3.0 Modes in Optical Fibers

In this chapter, we look into a different aspect of optical waveguide theory. Having obtained the nature of the solutions, we determine the actual solutions. There are infinite solutions and each is called a mode, the term being one used conventionally in waveguide theory. Modes are a mathematical conceptualization that helps us define, visualize and exploit the waveguide properties. They also have physical correlations. This analysis is largely based on that in Ref [2] and so explicit references will not be made at all places.

The two equations in (2.3.11) can be used together to formulate the characteristic equation of the step-index optical fiber. Such analysis has been presented by many authors [2, 3, 4, 6] and we reproduce here the final result in one of the many forms from [2].

$$
\begin{aligned}
(\mathrm{A}-\mathrm{B})(\varepsilon_1\mathrm{A}-\varepsilon_2\mathrm{B}) &= n^2\left(\frac{1}{u^2}-\frac{1}{v^2}\right)\left(\frac{\varepsilon_1}{u^2}-\frac{\varepsilon_2}{v^2}\right)\\
\mathrm{A} &= \frac{J'_n(u)}{uJ_n(u)}\\
\mathrm{B} &= \frac{H'_n(u)}{vH_n(v)}\\
u &= \kappa_1 a\\
v &= \kappa_2 a.
\end{aligned}
\tag{3.0.1}
$$

This eigenvalue equation contains all the information of the boundary conditions and the fields. Solutions to this equation will determine the eigenvalues u and v and these can be used in (2.3.13) to obtain the actual fields.

As is obvious, for a given a, ε_1, ε_2, and k (or λ), we can select any n and have infinite solutions. Each solution determines u, v and thus generates an unique field configuration. Each such field pattern is called a **mode**. Many such modes can exist simultaneously.

Replacing n by $-n$ does not change the characteristic equation and opens up a range of degenerate modes corresponding to the solutions. These will however differ in that they will have an opposite sense of rotation because of the $e^{jn\varphi}$ term in the field solutions. The solution for a particular choice of n can be associated with another mode number m assigned consecutively in order of appearance to the modes with the same n. This shall be explained later.

In optical fibers, we have total internal reflection as the guiding mechanism. For this, a propagating mode has a finite field in the core and an evanescent field in the cladding (κ_2 is imaginary).

3.1 Mode Nomenclature

Each different mode arises as a solution to the characteristic equation of the optical waveguide. This section describes the modes and their nomenclature.

We use n, the order of the Bessel functions as one of the means of classifying or naming the modes. This is called the *azimuthal mode number*. It is significant since it appears in the index of $e^{jn\varphi}$ and thus it gets its name. As previously mentioned, n has to be an integer since $e^{jn2\pi} = e^0$ only for integer n. If we observe the projection of the **E** vector on the transverse plane, then we can see that for $n = 0$, there is no azimuthal or rotational coefficient in **E** and **H**. The wave vector $\mathbf{u}_k$ is radial

and the equivalent ray for the wave passes through the axis and is always in a meridional plane. Less obvious is the fact that for higher n, the equivalent ray (along $\mathbf{u}_k$) never crosses the axis and the equivalent rays are skew [6].

Case 1: n = 0 [3]

For such cases, we get from (2.4.1)

$$(A - B)(\varepsilon_1 A - \varepsilon_2 B) = 0. \tag{3.1.1}$$

If the first term is zero, we have field solutions with ($E_z = 0$) and the **E** vector is in the transverse plane. These modes are termed transverse electric or TE_0 modes with the subscript $n = 0$. Correspondingly, if the second term is zero, we have ($H_z = 0$) and the **H** vector is in the transverse plane and these are termed TM_0 modes. As noted before, these modes correspond to meridional rays.

Case 2: n > 0 [2]

The characteristic equation can be rewritten as a quadratic equation as under.

$$A = \left(\frac{\bar{\varepsilon}}{\varepsilon_1}\right)B \pm P$$

$$P^2 = \left\{\left(\frac{\Delta\varepsilon}{\varepsilon_1}\right)^2 B^2 + n^2\left[\left(\frac{1}{u^2}\right) - \left(\frac{1}{v^2}\right)\right]\left[\left(\frac{1}{u^2}\right) - \left(\frac{\varepsilon_2}{\varepsilon_1 v^2}\right)\right]\right\} \tag{3.1.2}$$

$$\bar{\varepsilon} = (\varepsilon_1 + \varepsilon_2)/2\,,\ \Delta\varepsilon = (\varepsilon_1 - \varepsilon_2)/2.$$

For $n > 0$, we have hybrid modes where $E_z \neq 0$, $H_z \neq 0$ [2]. Field solutions for such modes become more complex and approximations have to be made for analysis. Note that the quadratic equation above is really two equations because of the $\pm$ sign. If we select the + ve sign, then we get modes which are conventionally termed EH_n modes. On the other hand, the -ve sign generates what are called the HE_n modes. Physical significance of these names arises from considerations of the transverse fields. The *HE* fields are more H-like and the *EH* fields are more E-like, which is to say that the transverse fields are dominated by the H or the E fields respectively. The same equation

can be used for $n = 0$ and as can be expected, the EH_0 modes are the TE_0 modes and the HE_0 modes are the TM_0 modes..

We defined α in (2.3.5) as a ratio involving the magnitudes of the fields E and H and can expect field dominance to be related to α. Without proof we write from [2]

$$\alpha = \frac{n}{A - B}\left[\left(\frac{1}{u^2}\right) - \left(\frac{1}{v^2}\right)\right]. \tag{3.1.3}$$

$|\alpha| < 1$, for *HE* modes
$|\alpha| > 1$, for *EH* modes

Thus, for EH modes, the axial component of the H-field is larger and the transverse component of the E-field is dominant.

The reader may recall that n can be replaced by $-n$ and we would still satisfy all equations. This suggests a degenerate orthogonal mode with an opposite sense of rotation. If $n < 0$, then α is positive for HE modes and negative for EH modes. There are other aspects of the rotational terms presented in 3.3 and the interested reader is referred to Ref [2] for a quantum mechanical interpretation.

3.2 Mode Cutoff Conditions

We need to have an evanescent wave in the cladding for guidance so as to prevent the radiation of power away from the core. A mode will not be bound to the core if the cladding field is not evanescent. It would be detached from the core-clad boundary and radiate power away from the core. We term the mode to be cut off and not supported in such cases. This condition is characterized by $\kappa_2 = 0$. Modes have a second subscript, the *radial mode number m* assigned in order of appearance as $|\kappa_2|$ is made greater than zero. Remember that κ_2 is imaginary for bound modes.

We shall see later that m influences the number of radial maxima in the intensity pattern of the mode. The cutoff conditions for different modes are given below [3].

$$\begin{array}{ll} TM_{0m}, TE_{0m} & J_0(u) = 0 \\ HE_{1m} & J_1(u) = 0 \\ EH_{nm}, n \geq 1 & J_n(u) = 0,\ u \neq 0 \\ HE_{nm}, n \geq 2 & \left(n_1^2/n_2^2 + 1\right)J_{n-1}(u) = uJ_n(u)/(n-1) \end{array} \tag{3.2.1}$$

The above conditions define $u = u_c$ at cutoff. For $u > u_c$, the mode is supported. So as u increases, more and more modes begin to be supported. We can relate this to the fiber parameters. At cutoff, we can use (2.1.12) to write

$$\begin{aligned} u_c = \kappa_1 a = a\sqrt{k_1^2 - h_1^2} &= a\sqrt{k_1^2 - k_2^2} \\ = ak\sqrt{n_1^2 - n_2^2} &= \left(\frac{2\pi a}{\lambda}\right)(NA) = V_c. \end{aligned} \tag{3.2.2}$$

For a mode to be supported we need

$$V > V_c = u_c. \tag{3.2.3}$$

The u_c parameter can be written in general for all modes except the HE_{nm}, $n \geq 2$ modes where knowledge of the ratio n_1/n_2 is needed. We assume for our applications, $n_1/n_2 = 1.002$. Then we have the cutoff conditions on V for some lower order modes as under.

Mode	u_c
HE_{11}	0.0
TM_{01}, TE_{01}	2.405
HE_{21}	2.42
HE_{12}, EH_{11}	3.83
HE_{31}	3.86
EH_{21}	5.14

The propagational constant h varies from k_2 to k_1 as a mode goes from cutoff to far-from-cutoff. The actual value of the propagation constant can be got by solving the characteristic equation. This can be done only by numerical methods.

The relation between h and V for a 9/125, NA = 0.1, V = 4.46 at 633 nm optical fiber was plotted by solving the equation numerically From above, we can see that only the first seven modes are supported for $V < 5$. This is depicted as a plot of h with V in Figure 6 on page 57.

The normalized propagation constant b is defined as

$$b = \frac{h^2 - k_2^2}{k_1^2 - k_2^2}. \tag{3.2.4}$$

The plot of h v/s V can be used to represent the relation of b v/s V. Since the fiber is weakly guiding, this b-V relation holds true for all optical fiber waveguides that satisfy the weakly guiding approximation ($n_1 \cong n_2$) [5].

3.3 Mode Field Expressions

Using the equations we have developed till now, we can, if desired, obtain the field expressions for any mode. The exact solutions are very complex.

If $U_\pm$ are the roots of $J_{n\pm1} = 0$, then, far from cutoff, taking $q = |v| \cong V$, we have in a first-order approximation,

$$u_\pm = U_\pm \left\{ 1 - \left(\frac{\bar{\varepsilon}}{\varepsilon_1 V} \right) \left(1 \mp \left[\frac{(2n \pm 3)\bar{\varepsilon}}{8\varepsilon_1 V} \right] \right) \right\}. \tag{3.3.1}$$

Using

$$h_{\pm} = \sqrt{(k_1^2 - \kappa_1^2)} \cong k_1 \left[1 - \left(\frac{\Delta\varepsilon u_{\pm}^2}{\varepsilon_1 V^2} \right) \right] \tag{3.3.2}$$

the individual mode parameters can be obtained now that we know u and h. We shall not be looking into the particular solutions. Extensive tabulations of exact mode expressions are available in [6]. However, since we are particularly interested in some EH and HE modes, we reproduce the following approximate expressions for fields far from cutoff derivable from (3.3.1) [2]. For EH_{nm} modes,

$$\begin{aligned} E_+ &\cong [2 + (\Delta\varepsilon u_+^2 / n\varepsilon_1 V)] A J_{n+1}(u_+ \rho / a) e^{j(n+1)\varphi - jh_E z + j\omega t} \\ E_- &\cong (\Delta\varepsilon u_+^2 / n\varepsilon_1 V) A J_{n-1}(u_+ \rho / a) e^{j(n-1)\varphi - jh_E z + j\omega t} \\ H_{\pm} &\cong j\sqrt{(\varepsilon_1/\mu)}\, E_{\pm}. \end{aligned} \tag{3.3.3}$$

For the HE_{nm} modes, we have [2]

$$\begin{aligned} E_- &\cong [2 + (\Delta\varepsilon u_-^2 / n\varepsilon_1 V)] A J_{n-1}(u_- \rho / a) e^{j(n-1)\varphi - jh_H z + j\omega t} \\ E_+ &\cong (\Delta\varepsilon u_-^2 / n\varepsilon_1 V) A J_{n+1}(u_- \rho / a) e^{j(n-1)\varphi - jh_H z + j\omega t} \\ H_{\pm} &\cong \pm j\varepsilon_1/\mu E_{\pm}. \end{aligned} \tag{3.3.4}$$

Note the duality between the HE and EH modes and the swapping of rotational charactersitics. Since $\Delta\varepsilon$ is small, the E_+ and E_- fields are dominant in the EH and HE modes respectively. This gives us another distinction between the two types of modes. For $n > 0$, the dominant polarization (E_+ for EH and E_- for HE) rotates opposite to the φ component in HE modes whereas that of the EH modes rotates in the same direction. The rotational behaviour of the $EH_{p-1,m}$ and $HE_{p+1,m}$ is thus similar. The propagational constants of these modes depend upon $u_{\pm}$ which differ only in the second order for our approximation [2]. Thus, these modes are near-degenerate because of the propagational constants being almost the same.

For weakly guiding fibers, $\Delta\varepsilon$ is very small and the modes can be considered degenerate. This result is very significant since such modes can be combined to form sets of linearly polarized modes [5].

The small difference in the propagational constants can however have some very interesting effects on the mode combination patterns as we shall see in the next chapter.

In the following sections, we shall consider the intensity patterns resulting from mode combinations.

3.4 Mode Combinations

The different modes in an optical fiber interfere with each other to form combinations. Note that only if the E-fields have components along the same direction will there be constructive or destructive mixing. Thus, the components that are polarized orthogonally like the LCP and RCP do not interfere in the real sense. The intensities simply add up. Only like polarized components can exhibit destructive interference causing interesting patterns.

The radiation patterns of the mode patterns can be observed in the near-field or far-field zones. At the fiber output endface, the mode fields and intensity pattern will be affected by the truncation of the ideal infinite cylinder. If we neglect the reflection and truncation effects, the radiation patterns can be related directly to the mode patterns like an aperture field radiation. Near and far-field observations of the radiaiton patters have been reported in the literature [2,4]. We shall consider the relation later. At this point, we note that, close to the axis, the radiation pattern has a definite correlation with the mode pattern.

We shall consider approximate cases of $EH_{k-1,m}$ and $HE_{p+1,m}$ modes with their degenerate counterparts. The reason for analysing these combinations is the convenient grouping arising from the near-degeneracy for k = p. For $|k,p| > 1$, we can describe the behaviour of the EH modes as (ignoring magnitudes),

$$
\begin{aligned}
EH_{k-1,m} &: E_+ \cong J_k(U\rho/a)e^{j(k\varphi+\omega t-h_E z+\psi)} \\
&: E_- \cong 0 \\
EH_{-(k-1),m} &: E_- \cong J_k(U\rho/a)e^{j(-k\varphi+\omega t-h_E z+\psi)} \\
&: E_+ \cong 0 \\
HE_{p+1,m} &: E_- \cong J_p(U\rho/a)e^{j(p\varphi+\omega t-h_H z)} \\
&: E_+ \cong 0 \\
HE_{-(p-1),m} &: E_+ \cong J_p(U\rho/a)e^{j(-p\varphi+\omega t-h_H z)} \\
&: E_- \cong 0,
\end{aligned}
\tag{3.4.1}
$$

where ψ is the random carrier phase. The behaviour of H in all these cases is

$$H_\pm = \pm jE_\pm. \tag{3.4.2}$$

Using (2.3.16), the intensity is given by

$$S_z = (1/4)\ \mathrm{Re}\,[j(E_+H_+^* - E_-H_-^*)]. \tag{3.4.3}$$

Remember that U is the mth root of $J_p(x) = 0$. For each of the above modes (and for all modes with radial number m), the intensity pattern is circularly symmetric with m maxima. If the two degenerate modes are combined this will still be the case because the two circular components are orthogonal in power and there will be a simple addition of intensities. Other 'cross-polarized' combinations have interesting effects.

Assuming that the magnitudes are the same and $J_k \cong J_p = J$, we write for $EH_{k-1,m} + HE_{-p-1,m}$,

$$
\begin{aligned}
S_z &\cong (1/4)[J_k^2J_p^2 + 2J_kJ_p\cos\{(k+p)\varphi - D\}] \\
&\cong J^2\cos^2\{[(k+p)\varphi - D]/2\} \\
D &= (h_E - h_H)z - \psi.
\end{aligned}
\tag{3.4.4}
$$

and for $EH_{k-1,m} + EH_{-k+1,m} + HE_{-p-1,m} + HE_{p+1,m}$, we get

$$
\begin{aligned}
S_z &\cong (1/2)[J_k^2 + J_p^2 + 2J_kJ_p \cos D \cos\{(k + p)\varphi\}] \\
&\cong J^2 \cos^2\{(k + p)\varphi/2\} \cos^2\{D/2\} + \sin^2\{(k + p)\varphi/2\} \sin^2\{D/2\} \\
D &= (1/2)\{(h_E - h_H)z - \psi\}.
\end{aligned}
\tag{3.4.5}
$$

There is an occurrence of nodal lines since the intensity goes to zero at specific values of φ . In fact, there are $2p$ such nodes at regular intervals. For the latter case, there can also be situations where the nodes vanish. This effect will be discussed in more detail for specific cases in Chapter 4. Note that for a fixed point on the pattern, say, $\varphi = 0$, we have from (3.4.4) and (3.4.5),

$$
S_z = J^2 \cos^2\{D/2\}. \tag{3.4.6}
$$

D can be evaluated if the difference between the propagation constants is known. (3.3.3).

3.5 *Mode Patterns*

The radiation field of an aperture is, in general, a very complex problem. The correlation of the far-field patterns back to the fields at the aperture may not be unique. Besides, the mode fields at the aperture are affected by the truncation of the waveguide and reflections from the endface. Observation of the near-field pattern neccesitates the physical proximity of measuring equipment (a lens) and this distorts the field itself. However, for non-exact solutions close to the axis, we can ignore many of these non-idealities. We will not attempt to obtain the complicated radiaton fields of the already complex mode fields. We outline a brief qualitative discussion here.

The radiation fields are obtained by considering the fields at the fiber endface as radiating elements. Far from cutoff, there is a principal maximum at a half-angle $\theta_{max} \cong \sin^{-1}[(k_1/k_0) \sin \theta_1]$, where θ_1 is the angle at which a plane wave composing the mode field strikes the glass-air interface. The

most important result is that for a radial mode number m , there are $m - 1$ maxima between $\theta = 0$ and $\theta = \theta_{max}$. For $m = 1$, there are not any maxima within the main pattern. Close to the axis, the radiation pattern for these modes are similar to the near-field patterns and the mode patterns [2,4]. Far from the axis, there will be a train of maxima and minima arising from the diffraction effects. In all cases except the HE_{1m} modes, there is a null in the forward direction. The HE_{1m} modes however, have a maximum in the forward direction. As a mode nears cutoff, the principal maxima move closer to the axis to fill up the null in the center. Remember that all individual mode intensities are circularly symmetric. The symmetry of mode patterns is preserved in the radiation pattern for the low-order modes.

Based on results in the previous section, we can qualitatively study the mode patterns and their behaviour.

1) $EH_{11} + HE_{21}$ (including degeneracies)

The intensity pattern for this combination can be studied more conveniently by studying $EH_{11} + HE_{-21}$. The general case with the degenerate cases is similar. The intensity pattern is

$$S_z = J^2 \cos^2\{(3\varphi - D_1)/2\} \tag{3.5.1}$$

The random phase in $D = (h_E - h_H)z - \psi$ doesn't really affect the intensity behaviour and it can be chosen to be zero for convenience. For a fixed z, say $z = 6N\pi$, we have a three lobed intensity pattern. This is illustrated in Figure 8 on page 59. Considering all the modes we get a little more complex behaviour since the three lobed pattern appears periodically in z whenever cos D or sin D becomes zero.

2) $EH_{11} + HE_{31}$

In this case,

$$S_z = J^2 \cos^2\{(2\varphi - D_2)/2\} \tag{3.5.1}$$

The above observations hold for this case too. The difference, however is that we have a four lobed pattern as illustrated in Figure 9 on page 60. In both the cases, as z is varied, we should see a rotation of the pattern since the nodal lines will apppear at different points.

3) $TE_{01} + HE_{21}$

In this case, we would have a two lobed pattern depicted in Figure 7 on page 58described by

$$S_z = J^2 \cos^2\{\varphi - D_3/2\} \tag{3.5.3}$$

Since $m = 1$ in these cases, there is one radial maximum in the intensity. The intensity is zero at the core-cladding interface. of the particular cases are also illustrated. Note the circular polarization varying in azimuth (different for the *HE* and *EH* modes). The *TE* and *TM* modes have no degenerate counterparts since $n = 0$. One sided arrow-heads are rotating E-vectors while two-sided ones are linearly polarized. Nodal lines appear just as predicted in the previous section. The phase factor D_i in all the above cases depends directly on the propagation constant difference which can be got from Figure 6 on page 57. The modulation of intensity due to the change in D or z will be examined closely in Chapter 4.

Identification of mode patterns can be done by comparison with photographs in the literature. A simple representation of far-field patterns is given in Figure 10 on page 61. The hatched lines indicate intensity and solid lines, whether circular or radial, indicate null intensities. The radial maxima and nodal lines are clearly represented. These do not, however represent the mode fields directly. Note the presence of a null in the forward direction except in the HE_{1m} cases.

To set up such field patterns in an optical fiber, it is essential that the respective modes be excited. Different modes and patterns can be excited by launching light at different angles to the axis. Another technique is to employ spatial filtering at the input to create suitable diffraction field patterns that maximize excitation of specific modes. These methods are discussed extensively in Ref [2]. We shall analyze the effects of mode modulation on mode combinations in the next chapter.

4.0 Mode-Mode Interference

In the previous chapters, we modelled the optical waveguide and analyzed the modal field solutions for lightwave propagation. As mentioned before, modal domain sensors utilize mode mode interference as a sensing mechanism. In this chapter, we shall present a theoretical basis for the mode modulation effects that we have seen experimentally.

First, we consider phase modulation in optical fibers since all interference phenomena involve phase effects.

4.1 Phase modulation in optical fibers

We have a general field solution for the transverse field of a propagating mode as

$$\begin{aligned} \mathbf{E} &= \mathbf{E}\,(\rho, \varphi) e^{jhz} \\ &= |\,\mathbf{E}(\rho, \varphi)\,|\, e^{jhz + j\Psi} \mathbf{u}_e. \end{aligned} \tag{4.1.1}$$

The phase Φ of the wave is given by

$$\Phi = hz + \psi_0 \tag{4.1.2}$$

where h is the longitudinal propagation constant and ψ_0 is the initial phase $\Phi(z)|_{z=0}$. This phase Φ is not be confused with the azimuthal angle φ . The initial phase ψ_0 is included for generality and we will drop it for initial calculations where it is not significant. We will insert it again as a random phase term later on.

Due to a given disturbance S (strain in our experiments), the phase Φ is modulated as under.

$$\begin{aligned} \Delta\Phi &= h(\Delta z) + L(\Delta h) \\ &= h\left(\frac{dz}{dS}\right)S + L\left(\frac{dh}{dS}\right)S. \end{aligned} \tag{4.1.3}$$

The first term in (4.1.3) depends essentially on the geometry of the fiber and the perturbing parameter.

For the specific case of axial (longitudinal) strain, ε_z , we write

$$\begin{aligned} \Delta z &= \varepsilon_z L \\ L &= \text{ length of interaction.} \end{aligned} \tag{4.1.4}$$

The variation of h with respect to the strain depends on the electro-optic and dimensional effects. We can expand Δh as [8]

$$\begin{aligned} \Delta h &= \left(\frac{dh}{dn}\right)\Delta n + \left(\frac{dh}{dD}\right)\Delta D \\ \text{where } n &= \text{ refractive index} \\ h &= \text{ longitudinal propagation constant} \\ D &= \text{ diameter of the core.} \end{aligned} \tag{4.1.5}$$

The change in the refractive index due to strain is given by [8]

$$\Delta n = -\frac{n^3}{2}[\varepsilon_z(1-\mu)P_{12} - \mu\varepsilon_z P_{11}]$$

ε_z = axial strain

μ = Poisson's ratio

P_{11}, P_{12} = Photoelastic constants. (4.1.6)

Typically, for optical fibers, $n_1 \cong n_2 = n_{eff}$ and so we write

$$\frac{dh}{dn} \cong k = \frac{2\pi}{\lambda_0}. \tag{4.1.7}$$

For the second term, we get [8]

$$\Delta D = \mu\varepsilon_z D$$

$$\frac{dh}{dD} = \frac{V^3}{2hD^3}\frac{db}{dV} \tag{4.1.8}$$

where b = normalized propagational constant

The variation of b with V for weakly guiding fibers is shown in Figure 6 on page 57. We can thus write for the strain induced phase change per unit strain per unit length,

$$\frac{\Delta\Phi}{\varepsilon_z L} = h - \frac{hn^2}{2}[(1-\mu)P_{12} - \mu P_{11}] + \frac{V^3\mu}{2hD^2}\frac{db}{dV}$$

$$= h - hA + \frac{B}{h}\frac{db}{dV} \tag{4.1.9}$$

where A, B = constant for all modes

For $V = 4.5$, $db/dV \cong 0.25$ (from -- Figure id " unknown --refid=bV3). Taking typical values $\mu = 0.25$, $D = 9\,\mu m$, and $h = 1.45 \times 10^7\ m^{-1}$, we get

$$A = 0.13$$

$$B = \frac{V^3\mu}{2D^2} = 1.407 \times 10^{11}\ m^{-2}.$$

Thus we have for the above specified fiber

$$\frac{\Delta\Phi}{\varepsilon_z L} \cong 1.45 \text{ x } 10^7 - 2.1 \text{ x } 10^6 + 2.4 \text{ x } 10^3 \text{ m}^{-1} \cong 1.24 \text{ x } 10^7 m^{-2}. \tag{4.1.10}$$

Though the third term is very small, we should be careful because we are going to consider differential phase effects and do not know before hand if the third term contribution is negligible. Having analyzed the phase modulation mechanisms due to strain, we now develop the theory of modal domain sensing based on differential phase modulation.

4.2 *Differential Phase Modulation*

For two different modes, we have two phases Φ_1 and Φ_2. The differential phase $\Phi_{12} = \Phi_1 - \Phi_2$ is the phase of one with respect to that of the other. Usually, a phase modulation results in the variation of both the phases as well as the differential phase. We can thus write

$$\begin{aligned} \Delta\Phi_{12} &= \{(\Phi_1 + \Delta\Phi_1) - (\Phi_2 + \Delta\Phi_2)\} - \Phi_{12} \\ &= \Delta\Phi_1 - \Delta\Phi_2. \end{aligned} \tag{4.2.1}$$

4.2.1 Axial strain

Substituting (4.1.9) in (4.2.1), we get the following expression for the differential phase per unit strain per unit length.

$$\begin{aligned} \frac{\Delta\Phi_{12}}{\varepsilon_z L} &= 0.87(h_1 - h_2) + B\left(\frac{1}{h_1}\frac{db}{dV}\Big|_{b=b_1} - \frac{1}{h_2}\frac{db}{dV}\Big|_{b=b_2}\right) \\ &\cong 0.87h_{12} - 1.407 \text{ x } 10^{11}\frac{h_{12}}{h_1 h_2} \end{aligned} \tag{4.2.2}$$

From Figure 6 on page 57 , we can say $h \cong 1.45 \times 10^7\ m^{-1}$. Thus, it is obvious that the second term in (4.2.2) can be neglected.

It is significant that the differential phase modulation due to strain depends only on the difference of the propagational constants. We thus write for two modes having propagation constants h_1 and h_2 with $h_{12} = h_1 - h_2$,

$$\Delta\Phi_{12} = 0.87(\Delta z)h_{12} \tag{4.2.3}$$

where $h_{12} = h_1 - h_2$ is typically obtained from a numerical solution of of the characteristic equation.

The intensity of the output depends on the terms described in (2.3.16). For more sensitivity, the mode combination that we select must preferably have a large differential phase coefficient h_{12} that converts efficiently to intensity modulation in such a manner that we can detect it easily. Note that

$$\frac{\Delta\Phi_{12}}{\Delta z} = 0.87h_{12} \leq 0.87k_0(n_1 - n_2). \tag{4.2.4}$$

The phase modulation for a dual beam interferometer is the absolute phase change $\Delta\Phi$ given by (4.1.9) and (4.1.10). So, the maximum sensitivity of a modal domain scheme can be related to that of a conventional dual-beam interferometer. For the same physical characteristics of the fiber and setup, we get

$$\frac{\Delta\Phi_{12}(\text{modal domain})}{\Delta\Phi(\text{MZI})} \leq \frac{2.59 \times 10^4}{1.24 \times 10^7} = O(10^{-3}). \tag{4.2.5}$$

This upper limit may not be attainable since the choice of mode combinations depends on the feasibility of exciting the relevent modes. Moreover, the differential phase modulation has to be demodulated to extract the information. This could either be simple intensity measurement or might need processing. To use this effect in a sensor, this demodulation must preferably be as simple as possible.

The sensitivity is definitely less than the absolute phase sensitivity of a fiber optic sensor. The advantages are the simplicity and ruggedness of a single fiber sensor with all its advantages of stability, common-mode rejection etc. We shall look at the effect of the differential modulation for particular cases.

4.3 *Mode Pattern Modulation*

The $HE_{11} + TM_{01}$ combination has been used in the past [12] to sense acoustic waves perturbing an optical fiber coil in water. The mode pattern in this case consists of two lobes.

We have observed some interesting rotational effects in a three-lobed mode pattern later identified later as arising from the $EH_{11} + HE_{21}$ mode combination. Such effects can been predicted by analysis of mode combinations and radiation patterns.

In a general case, if linearly polarized light is used to launch the modes, one would expect coupling of power to both the circular polarization components of the fields. However, for illustration purposes, let's consider the combination $EH_{11} + HE_{-21}$. The intensity is given by (3.4.4) as under.

$$I_z = J^2 \cos^2[(3\varphi - h_{12}z + \psi)/2.] \tag{4.3.1}$$

ψ is a random carrier phase and can be adjusted or allowed to come to any desired value. If it is zero, we can then see that for $z = 6N\pi/h_{12}$, $N = 0,1,2..$, we have a circular pattern with three nodal lines at $\varphi = (2p + 1)\pi/3, p = 0,1,2$. At $z = (6N + 1)\pi/h_{12}$, we have the three nodal lines shifted to $\varphi = 2p\pi/3, p = 0,1,2$. Thus, we see this interesting rotation effect arising due to h_{12} , the difference in the propagation constants.

Now, if we consider the general case of both the polarizations being launched, we have the combination $EH_{11} + EH_{-11} + HE_{31} + HE_{-31}$. The intensity in this case is given by (3.4.6) [2] and we reproduce it here.

$$I_z = J^2\{\cos^2(3\varphi/2)\cos^2(D/2) + \sin^2(3\varphi/2)\sin^2(D/2).\}$$

There is still rotation of nodal lines but it is more complex. The polarization states in the four lobes are different from before. Taking $\psi = 0$, we get three nodal lines whenever $\cos h_{12}z$ or $\sin h_{12}z$ becomes zero.

If the optical fiber is subjected to an a phase modulating disturbance such as axial strain of ε_z, then, as seen before, only the h_{12} term is responsible for the differential phase modulation. This h_{12} appears conveniently in the mode intensity pattern. Let us see how this affects the intensity.

Fixing a point P(ρ, 0) on the output pattern, we get

$$\begin{aligned} I_z &= J^2\cos^2(D/2) \\ &= J^2\cos^2(h_{12}z - \psi)/2. \end{aligned} \tag{4.3.2}$$

Another interesting approach to the problem is to consider two carriers with different phase modulation.

$$\begin{aligned} E_1 &= E_0\cos(\omega_c t + \Delta\theta_1 + \psi) \\ E_2 &= E_0\cos(\omega_c t + \Delta\theta_2). \end{aligned}$$

The interference signal when detected by a square law detector (since a photodiode current relates to intensity) can be described as

$$i(t) = |A|\cos^2\{(\Delta\theta_{12} + \psi)/2\} \tag{4.3.3}$$

Thus, it is reasonable to expect that mode combinations should display the differential phase modulation as an intensity modulation due to mode-mode interference.

4.3.1 Axial Strain

For axial strain ε_z, $\Delta z = \varepsilon_z L$. The initial value of z, z_i only creates an offset and without loss of generality, we can write from (4.3.2)

$$I_z = J^2 \cos^2\{(h_{21}\varepsilon_z L - \psi)/2\}. \tag{4.3.4}$$

Again, ψ is a random term and the response can be optimized by launching conditions. Taking $\psi = 0$ since it is only an offset, we have for $\Delta z = Kt$ (linear ramped strain),

$$I_z = J^2 \cos^2(Kh_{12}t/2). \tag{4.3.5}$$

The intensity is maximum for $t = 0$ and minimum for $t = \pi/Kh_{12}$. The period T for this sinusoidal variation is given by

$$\begin{aligned} T &= 2\pi/Kh_{12} \\ \text{where } K &= \text{ rate of strain.} \end{aligned} \tag{4.3.6}$$

4.3.2 Generalized Axial Strain

Strain could be any function of time, in general. We can split any function into its sinusoidal components. So we assume a sinusoidal variation of strain. Thus, z is given by

$$\begin{aligned} z(t) &= z + L\varepsilon_z(t) = z + L\varepsilon_0 \sin \omega t \\ &= z + z_0 \sin \omega t. \end{aligned} \tag{4.3.7}$$

The initial z can be ignored since it can be adjusted to any desired point by straining the fiber suitably. So we have the general intensity expression of (4.3.2) with $D = h_{12}z_0 \sin \omega t - \psi$. For $\varphi = 0$,

$$I_z = J^2 \cos^2(D/2)$$
$$D = h_{12} z_0 \sin \omega t - \psi \tag{4.3.8}$$

We can write

$$\begin{aligned} \cos^2(D/2) &= (1/2)\{1 + \cos[h_{12} z_0 \sin \omega t - \psi]\} \\ &= (1/2)[1 + \cos(h_{12} z_0 \sin \omega t) \cos \psi + \sin(h_{120} \sin \omega t) \sin \psi]. \end{aligned} \tag{4.3.9}$$

The transcendental arguments give rise to a an infinite series with Bessel coefficients.

$$\begin{aligned} \cos(h_{12} z_0 \sin \omega t) &= J_0(h_{12} z_0) + 2 \sum_{1}^{\infty} J_{2k}(h_{12} z_0) \cos 2k\omega t \\ \sin(h_{12} z_0 \sin \omega t) &= 2 \sum_{0}^{\infty} J_{2k+1}(h_{12} z_0) \sin(2k + 1)\omega t. \end{aligned} \tag{4.3.10}$$

Thus,

$$\begin{aligned} I_z = \; & [1 + 2J_0(h_{12} z_0) \cos \psi \\ & + 2J_1(h_{12} z_0) \sin \psi \sin \omega t \\ & + 2J_2(h_{12} z_0) \cos \psi \cos 2\omega t .....]/2 \end{aligned} \tag{4.3.11}$$

Thus, to obtain the original signal we need to adjust the relative carrier phase to $\pi/2$. This is possible by adjusting the launching conditions. There could be a random variation in this which could decrease the sensitivity or cause fading as reported in [11]. The argument of the Bessel functions,

$$\begin{aligned} h_{12} z_0 &= h_{12} \varepsilon_0 L \\ &= h_{12} \Delta z. \end{aligned} \tag{4.3.12}$$

In our experiments with $EH_{11} + HE_{21}$,

$$\begin{aligned} |h_{12}| \varepsilon_0 L &= (1.2 \times 10^4)(1 \times 10^{-4})(0.16) \\ &\cong 0.19 \end{aligned} \tag{4.3.13}$$

For 0.19, except for J_0 all Bessel functions are near zero. $J_0 \cong 1$. However, for longer lengths of interaction, the relative magnitudes might be different. For our case,

$$I_z = A \sin\psi \sin\omega t \tag{4.3.14}$$

We have analyzed a specific mode combination. The results we have obtained by direct analysis agree with the the generalized results of analysis for two general modes done in the past [10,11]. The main points are,

- The prediction of multiples of the fundamental frequency
- The dependence of the magnitudes of the harmonics on the modulation, strain and length. The response is very clear, for small strain.
- The occurrence of the random carrier phase which needs to be adjusted or tuned for suitable output

4.3.3 Other Effects : Triple Transit

In the previous sections, we reviewed phase modulation and differential phase modulation in optical fibers. We applied this to mode-mode interference and saw its effect on mode pattern intensity.

The modulation of intensity due to modulation in the phase could arise from other effects also. Particularly, there could be interference between a mode and its reflected component making its third transit through the sensing region [11]. We could call this the triple transit echo. Single fiber interferometers can be based on this triple transit echo and can be improved by maximizing the reflections at the endfaces. Due to a mode (or a mode combination) travelling the region of interaction thrice, we can get interference between a modulated mode

$$E_t e^{j\Delta\Phi t}$$

and its triply travelled counterpart

$$RE_t e^{j3\Delta\Phi - \psi}$$

Then we get intensity modulation as

$$\begin{aligned} I(t) &= RI_{\rho}(\rho)\cos^2 D \\ \text{where } D &= \Delta\Phi - \psi \end{aligned} \tag{4.3.15}$$

Note the doubling of the phase term. The magnitude of this effect is reduced due to reflection loss and attenuation and can be neglected [11].

5.0 Experiment

Most of the work reported in this thesis was initiated by experimental observations. As is typical with a scientific study, experiment and theory go hand in hand irrespective of which occurs first. In this case, some experiments were motivated after a hypothesis was formulated about the mode interference and mode pattern phenomena. The term *modal domain* was coined for work involving mode modulation and interference phenomena.

The primary perturbation mechanism in these experiments is strain. The choice of strain has three reasons.

- Strain causes changes in the length L, longitudinal propagational constant h and thus, the phase Φ of an optical fiber.
- Strain sensing is of major importance in structural applications, especially in aerospace, space and materials research.
- It is convenient to set up methods of straining an optical fiber.

The experiments are classified in the following manner.

1. Quasi-static ramped axial strain: This involved the application of axial strain without any bending effects. This strain is also quasi-static in the sense that it could be applied as a "DC strain" or quasi-statically varying strain using a direct fiber tension mechanism.

2. Vibrational strain: This involved the application of strain via the vibration of a cantilever beam to which the optical fiber was bonded.

The basic set-up is illustrated in Figure 11 on page 62. The primary effect used in the experiments is the redistribution of the far-field radiation (intensity) pattern of optical fiber due to strain. The optical fiber we used was designed for single-mode operation at 1300 nm. Measurements with a Photon Kinetics FOA-2000 Fiber Analyzer indicate a 9/125 μ, 0.1 NA fiber with a second mode cutoff wavelength of 1215 nm. Test results are shown in Figure 13 on page 64. At the operating wavelength of 633 nm, it had $V \cong 4.5$. Referring to section 3.2, this indicates that it can support (for $n_1/n_2 = 1.004$) the first seven modes HE_{11}, TE_{01}, TM_{01}, HE_{21}, EH_{11}, HE_{31} and HE_{12} .

The light source used was a Hughes 3221H-PC He-Ne laser with 1 mW linearly polarized output at 633 nm. Note that mode-mode interference techniques are possible only with coherent and stable light sources. The fiber was mounted on a tensile testing machine so that axial strain could be applied. Another part of the fiber was bonded to a cantilever beam so that it could be subjected to vibrating strain at the fundamental frequency of the beam. This is shown in Figure 12 on page 63. The detector was an in-house detector-amplifier based on a Hamamatsu Silicon photodiode. The detector output was fed into a Nicolet Explorer (204-A plug-in, 2081 option) digital storage oscilloscope which was interfaced to an IBM PC/XT on a IEEE-488 bus using a Metrabyte IEE-488 interface card. For frequency analysis, the data was uploaded to the IBM 3090 mainframe. Plots shown in this report were plotted on a Versatec electrostatic plotter using the SAS/GRAPH graphics package. The IMSL Fortran subroutines FFTRC were used for Fourier analysis. The characteristic equation for optical fibers was solved numerically on the same computer.

5.1 *Mode Pattern Observations*

The mode patterns were obtained by adjustment of the launch conditions and were observed on a screen/card in the far-field of the output end. A simple spring loaded xyz-tilt was used to position the fiber endface suitably. It was found that the tilt angle was a very crucial parameter and the higher order mode combinations were launched most efficiently when the fiber was tilted at a small angle.

For zero tilt, the HE_{11} mode was dominant. Other combinations observed were the two-lobed $HE_{11} + TM_{01}$, the three lobed $EH_{11} + HE_{21}$ and the four lobed $EH_{11} + HE_{31}$ This identification was based on results, sketches and pictures in the literature [2,7]. The problem of identifying modes based on observations in the far-field and analysis within the fiber is by no means a unique one nor a trivial one. But, we feel that such methods of identification are justified.

A very interesting phenomenon was the proximity of the three lobed and four lobed patterns as regards to adjustments of the tilt. These patterns would flip into the other one due to disturbances and maybe when strain was applied. When the experimental readings were taken, we could not observe the patterns at the same time. But later on, the author repeated the experiments and obtained the same results (the period in Figure 14 on page 65). The mode pattern was three-lobed when the results were taken again and this pattern manifested very distinct rotation at times whereas it was a complex redistribution rather than rotation at the other times. The highs and lows of the intensity pattern as the fiber was strained could be associated with the dark and bright areas of the pattern as it changed. (The amplifier had a negative gain).

Thus, it seems that our results pertain to the three lobed pattern. This confirms with observations made by colleagues [13]. The regularity of the output signal was directly related to the purity of launch of the mode combination.

We have worked with the four-lobed pattern also but it is not clear if the pattern shifted to other patterns. This uncertainty is not unique to this combination. Because of modal coupling, there is a redistribution of power in the modes and this affects the mode pattern nature. In all cases, the mode pattern had some non-idealities and results varied (sensor performance) depending on adjustments to the set-up.

Mode launching techniques have been studied in the past [2,7]. Simple methods like ours based on tilt of launch as well as more sophisticated techniques based on polarization and spatial filtering have been reported.

The detector was set up in such a way that it sampled the intensity of a small part of the pattern, usually a spot on one of the lobes. A small aperture was placed in front to achieve this local intensity monitoring. Thus we could monitor intensity changes at a point due to mode pattern modulation. The experiments themselves are described in the following sections.

5.2 *Quasi-Static Ramped Axial Strain*

The motivation for this experiment was to apply strain axially without any bending effects. It was felt that this could quantify the mode pattern modulation due to axial (or longitudinal) strain causing a change in length. The optical fiber was mounted in a tensile testing machine, the J.J. Lloyd T20,000. Special grips were used to prevent the slipping of fiber. The length of interaction was 190 mm. Force and displacement could be monitored simultaneously. Besides static strain, a very slowly varying, quasi-static strain could also be applied by setting a fixed displacement rate. This rate could be maintained accurately because the load torque on the motor due to the fiber was negligible.

Initially, the spatial filter was set at $\rho \cong a/2$ on a nodal line. Two tests were conducted.

1. The fiber was tensed with the application of different displacement rates 0.5 mm/min and 1.0 mm/min.

2. The fiber was tensed and released in the at the same rate to retrace the strain condition.

The displacement rates were low enough to simulate a quasi-static strain condition. Because of the way the experiment was set up, the resulting displacement created axial strain without any major bending effect of the sensing region. There was however increased pressure on the fiber at the grips, but we feel that the strain effect was dominant.

Figure 14 on page 65 shows the intensity detected by the photodiode for a displacement rate of 0.5 mm/min.

From (4.3.6), for a rate K, the 'beat' half-period of the intensity $T_{pp} = \pi/h_{12}K$. For $HE_{21} + EH_{11}$, we have from Figure 6 on page 57 that $h_{12} = 1.2 \times 10^4$. Thus

$$T_{pp} = \pi/(12000)(0.5 \text{ mm/min})$$
$$= 31.4 \text{ s}$$

From experiment, we get $t = 26$ s.

For the 190 mm length, the time axis could be related to strain. We get the strain rate as 4.386×10^{-5} /sec. Thus the intensity can be easily related to strain. The ***dynamic range*** for strain sensing is around 1140 μm/m. The smallest change detectable can be crudely measured from the stored waveform as being 15 dB below the maximum strain. This gives us the approximate ***strain sensitivity*** as 3.8×10^{-5}.

To check the retraceability of the system, we released the fiber exactly as above till it reached the initial point. This output is shown in Figure 15 on page 66. This process was repeated to confirm the effect.

To confirm the intensity modulation as being related to the displacement, we used a rate of 1 mm/min. The two intensity outputs are shown in Figure 16 on page 67. Note the relationship to the displacement rate which is doubled in the latter.

5.3 Vibrational Strain

In the same setup, we also bonded a part of the fiber to a cantilever beam. The beam was a steel blade (length = 16 cm, thickness = 0.65 mm) clamped at one end. The fiber was bonded to the surface as a loop so that it was not dangling. Thus, the distance of the fiber from the neutral axis was 0.325 mm. The cantilever was set into vibrations by starting off an initial displacement of 1 cm from the neutral axis at the tip. The cumulative strain on the fiber is given by [8]

$$\bar{\varepsilon} = 3da/2L^2, \tag{5.2.1}$$

where d = displacement and a = distance from neutral axis. Thus our initial strain at t = 0 is 1.9 x 10^{-4} and much less after the vibration begins to to damp.

The cantilever vibration was tested for two cases. The first was when the intensity was at a maximum (point A) in Figure 14 on page 65. The second was when the intensity was at a mean point (point B in Figure 14 on page 65). Just by observation of the intensity output from the quasi-static case, we expect that the second case B would have greater response and linearity than the first one. The time and frequency plots of the two cases are shown in Figure 17 on page 68 and Figure 18 on page 69. Note the higher magnitudes in the second case. The frequency spectrum from the

second case shows only a fundamental component at 16 Hz. The first case has distortion with the presence of multiple frequencies. Also note that the fundamental has a lower magnitude than the second multiple.

We shall discuss these results in the next chapter.

6.0 Results And Discussion

We can summarize the report as under. Chapters 2 and 3 presented optical waveguide theory with emphasis on mode field properties. The combinations of modes and the resulting patterns were discussed. Specifically, the $EH_{(k+1),m} + HE_{(p-1),m}$ combination was analyzed in detail. Chapter 4 addressed mode-mode interference. Phase modulation and differential phase modulations were described. Unique to this problem were the differential phase modulation mechanisms and their effect on intensity. Mechanisms of information demodulation were studied.

The experiments conducted are significant in the fact that they create axial strain without bending. Quasi-static ramped axial strain was applied. The sinusoidal behaviour of the intensity was as described by (4.2.3) was observed and experimentally verified. The retraceability test indicates the potential use of the mechanism in varying strain sensor schemes. Since the intensity behaviour was observed to be dependent on displacement and rate, we can connect the intensity and phase modulation effects. Thus, this experiment substantiates the mode-mode interference technique.

The theoretical and observed value of the beat-periods are in good agreement. It confirms our model of mode-mode interference based on differential phase modulation.

The occurrence of multiple harmonics for varying strain as indicated by the analysis is confirmed.. Note that the first cantilever test has more magnitude in the second multiple. This could be due to the random phase effect lending dominance to the even multiples term in (4.3.11). The variation of response magnitude and linearity with the bias point is very interesting. The results are what one would expect by observation of the transfer function. Since the experiments verify the effect of strain on the output, application of strain could be used as a control mechanism to tune the sensitivity of a system.

The mode combination that we have used can be easily launched. But it might be possible to obtain the advantages of modal domain techniques with other combinations. Breaking the degeneracy of the two HE_{11} modes to obtain differential modulation as in [9] could also be treated as a mode-mode interference scheme.

The only new demand from the system is the selective launching of modes and filtering of the output pattern. All this could be achieved by precise alignment of input positioners and filters at the output. Precise, fixed arrangements to couple light into selected modes or from sections of the output pattern, if implemented, could provide more stability to the mechanism. We are confirming our analytical results with experimental results. It must be kept in mind that this is valid only if our identification of the modes was right. This area needs more investigation since it is crucial for further work. To use the analysis, the mode combination has to be identified to some reasonable degree.

Modal domain methods are 2 to 4 orders less sensitive than absolute phase methods. However, there is an advantage of simplicity, common-mode rejection, no need of couplers or mirrors and thus offer ruggedness and simplicity of implementation. There is no doubt that this method can be used with advantage. The simplicity of the scheme has been demonstrated in sensing schemes to detect vibration [13] and stress waves in graphite-epoxy composites [14].

7.0 Conclusion

In conclusion, we outline what we have achieved here.

- Mode-mode interference in optical fibers has been explained starting from first principles. A model for mode-mode interference phenomena has been proposed based on differential phase modulation. The differential phase modulation is solely due to the difference in the propagation constants of the modes.

- The specific case of quasi-static ramped strain and varying strain has been discussed in detail for the EH + HE combination. Mechanisms of modulation have been investigated and a quantitative treatment of strain sensing has been presented. This was made possible by the numerical solution of the characteristic equation.

- The problem of mode pattern generation and identification has been addressed. Mode launching and radiation mechanisms are areas of potential interest that need to be studied further.

- A suitable experiment for the testing of modal methods has been devised and implemented. Experimental observations agree very well with the theoretical results thus confirming the model.

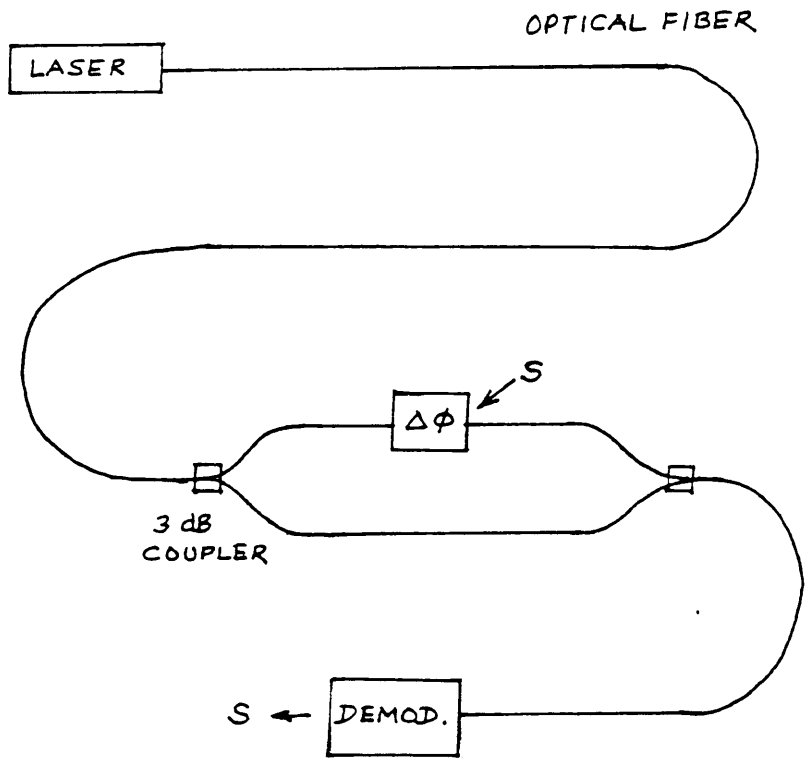

Figure 1. The Mach-Zehnder Interferometer: The intensity at the output depends on the phase of the light from the sensing arm with respect to that of the reference. Phase modulation in the sensing arm is demodulated at the output. This is the most sensitive type fiber optic sensor

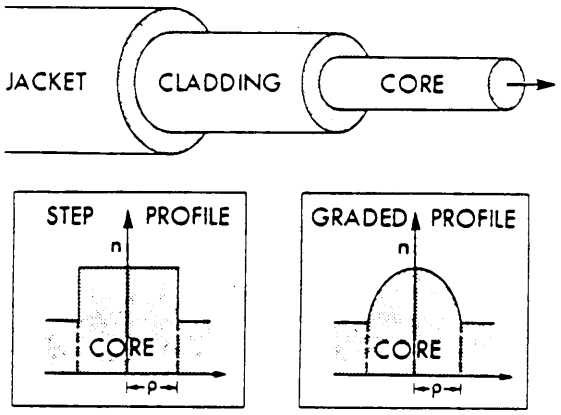

MULTIMODE FIBER	SINGLE-MODE FIBER
12.5 μm < ρ < 100 μm	2 μm < ρ < 5 μm
0.8 μm < λ < 1.6 μm	0.8 μm < λ < 1.6 μm
0.01 < Δ < 0.03	0.003 < Δ < 0.01

Figure 2. An optical fiber

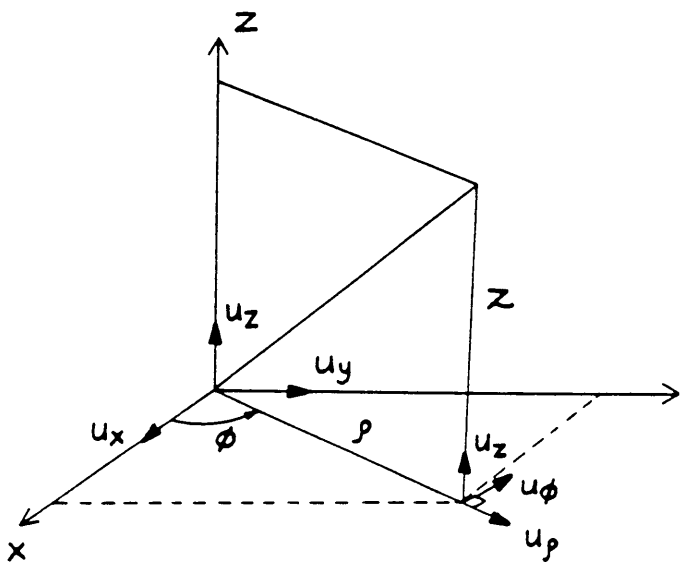

Figure 3. Cylindrical Coordinate System

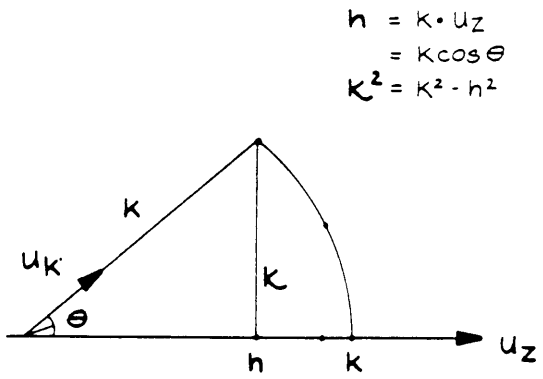

k = PROPAGATIONAL CONSTANT
h = LONGITUDINAL PROPAGATIONAL CONSTANT
κ = TRANSVERSE PROPAGATIONAL CONSTANT

Figure 4. **Propagational Constants:** k is the propagational constant, h, the longitudinal propagational constant and κ, the transverse propagational constant

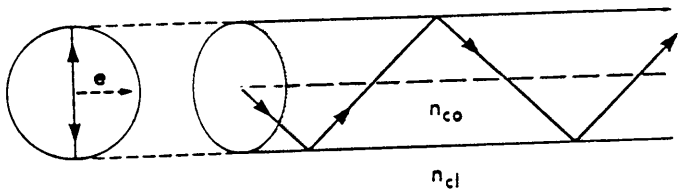

$n = 0$: MERIDIONAL RAY
TE_{om} , TM_{om} MODES

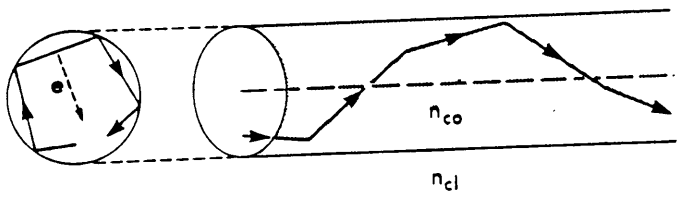

$n > 0$: SKEW RAYS
EH_{nm} , HE_{nm} MODES

Figure 5. **Ray trajectory for meridional and hybrid modes** Only for $n = 0$ we have the ray passing through the axis with no rotational component. These correspond to transverse modes. The skew rays ($n > 0$) correspond to hybrid modes. (From [6])

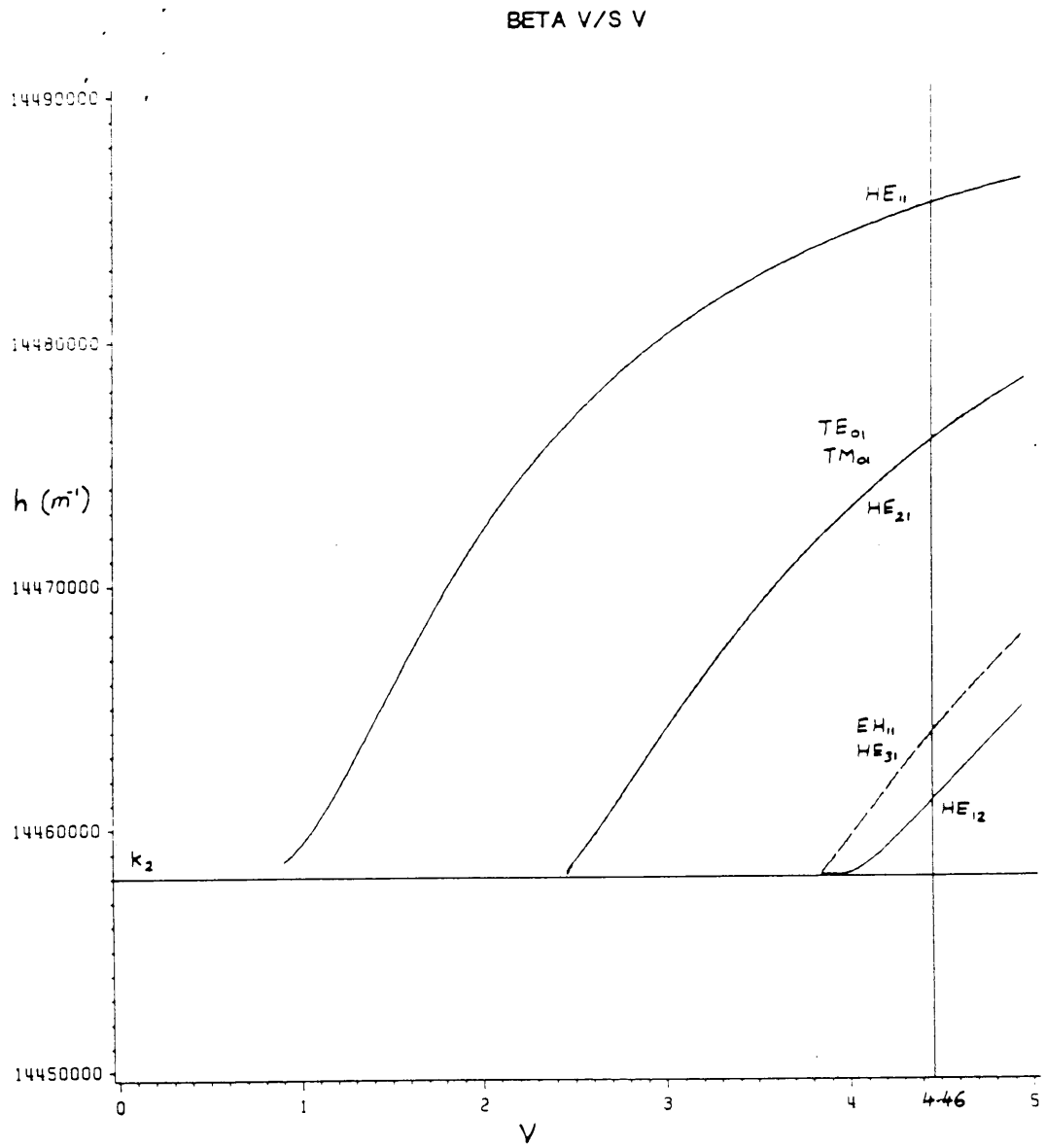

Figure 6. h vs V for low order modes: The longitudinal propagational constant plotted against V. Fiber parameters are 9.125 μ, 0.1 NA, n_1 = 1.46 and V = 4.46 at 633 nm.

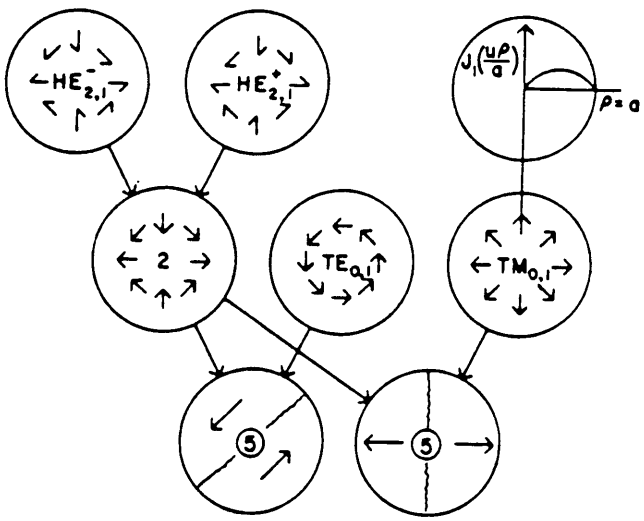

Figure 7. Mode fields inside an optical fiber: The orientation of the E vectors along the ring of maximum intensity are shown for TM_{01} + TE_{01} + HE_{21} . Solid lines are nodes. A one-sided arrow head is a circulating vector. Double-sided arrow heads correspond to linearly polarized fields. From [2].

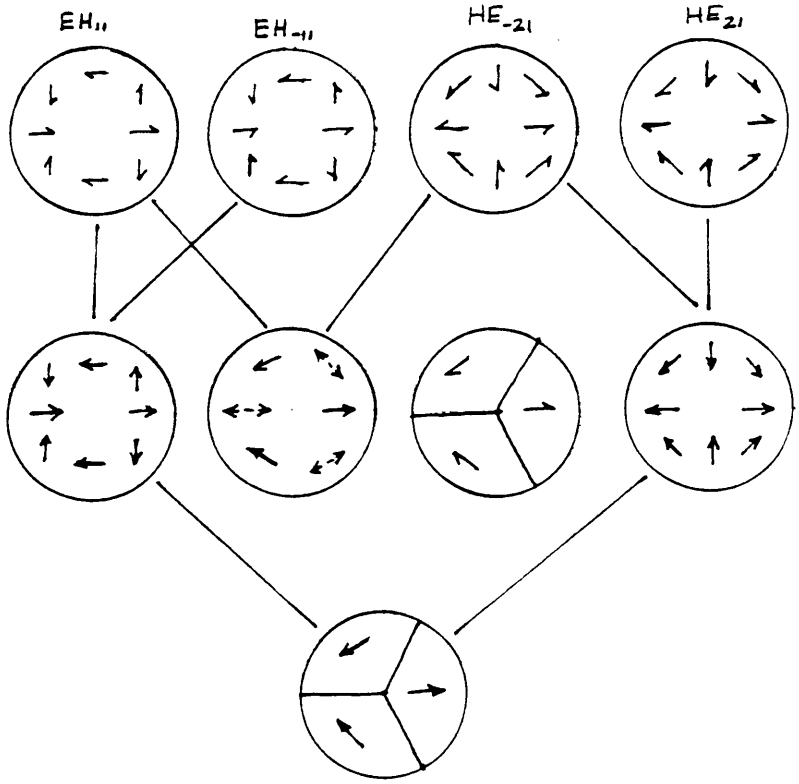

Figure 8. Mode fields inside an optical fiber: The orientation of the E vectors along the ring of maximum intensity are shown for $HE_{21} + EH_{11}$. Solid lines are nodes. A one-sided arrow head is a circulating vector. Double-sided arrow heads correspond to linearly polarized fields.

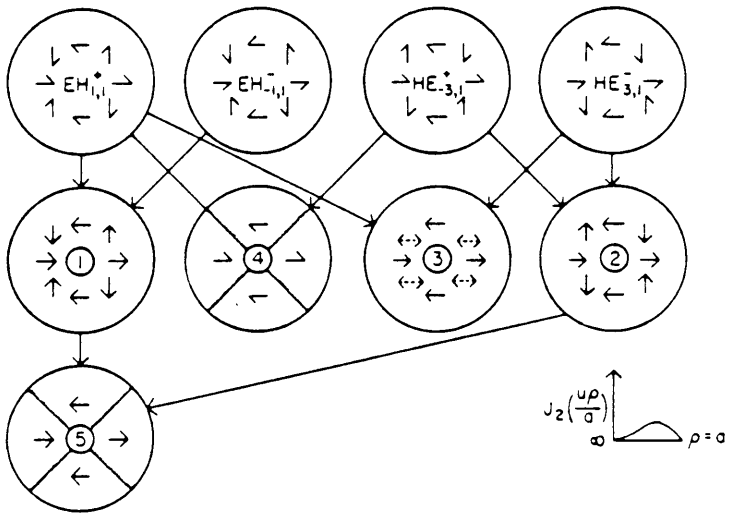

Figure 9. Mode fields inside an optical fiber: The orientation of the E vectors along the ring of maximum intensity are shown for $HE_{31} + EH_{11}$. Solid lines are nodes. A one-sided arrow head is a circulating vector. Double-sided arrow heads correspond to linearly polarized fields. From [2].

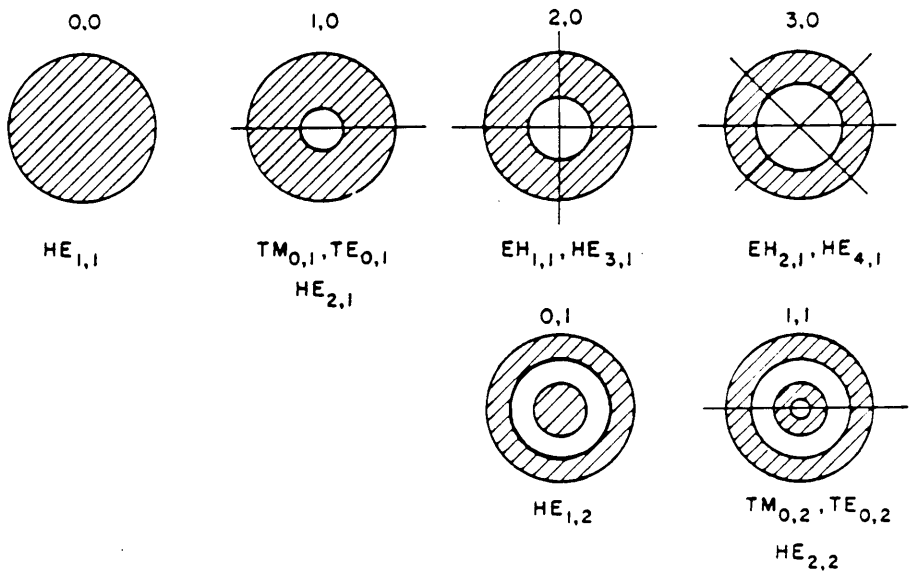

Figure 10. Identification of far-field mode patterns: Simple sketches for far-field radiation patterns. Shaded areas represent intensity. Solid lines, radial or circular are nodes. The patterns result from the coherent combination of the modes shown alongside. The second mode subscript indicates the number of radial maxima. Note the null in the forward direction for all modes except HE_{1m} From [2].

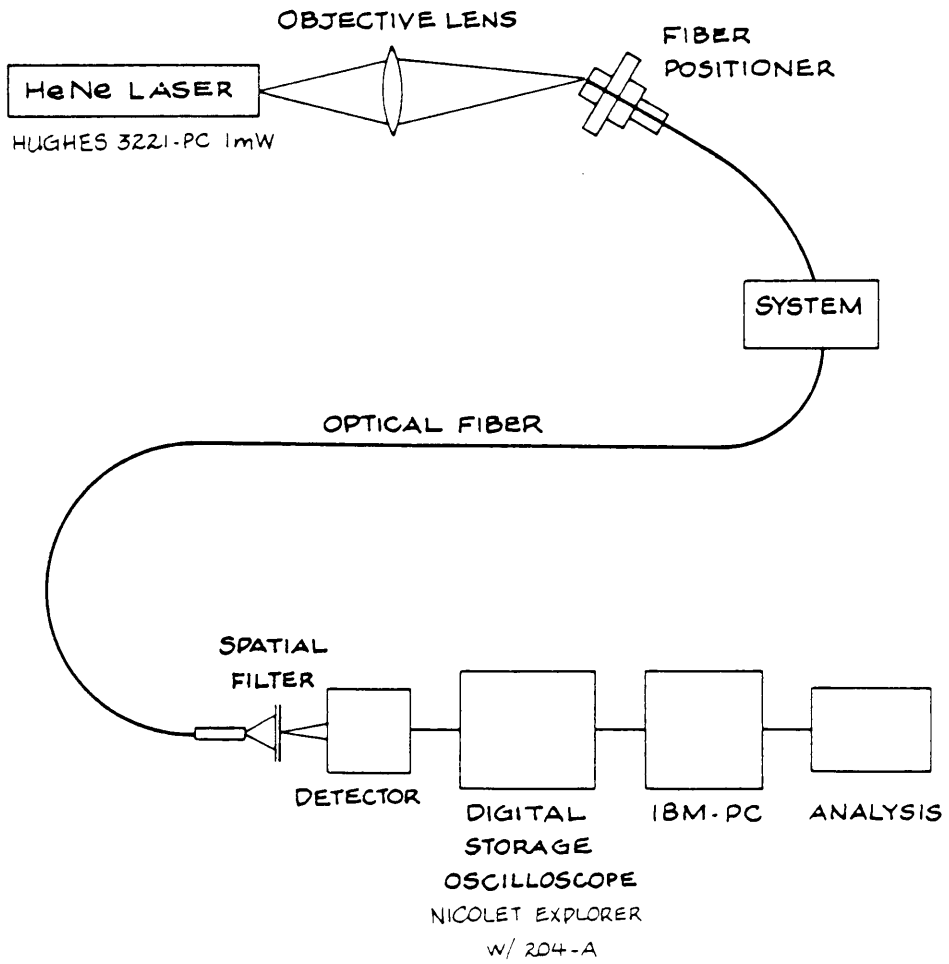

Figure 11. Experimental Setup: The arrangement at the output is to demodulate the differential phase modulation effect. In this setup, local intensity monitoring was implemented using a spatial filter.

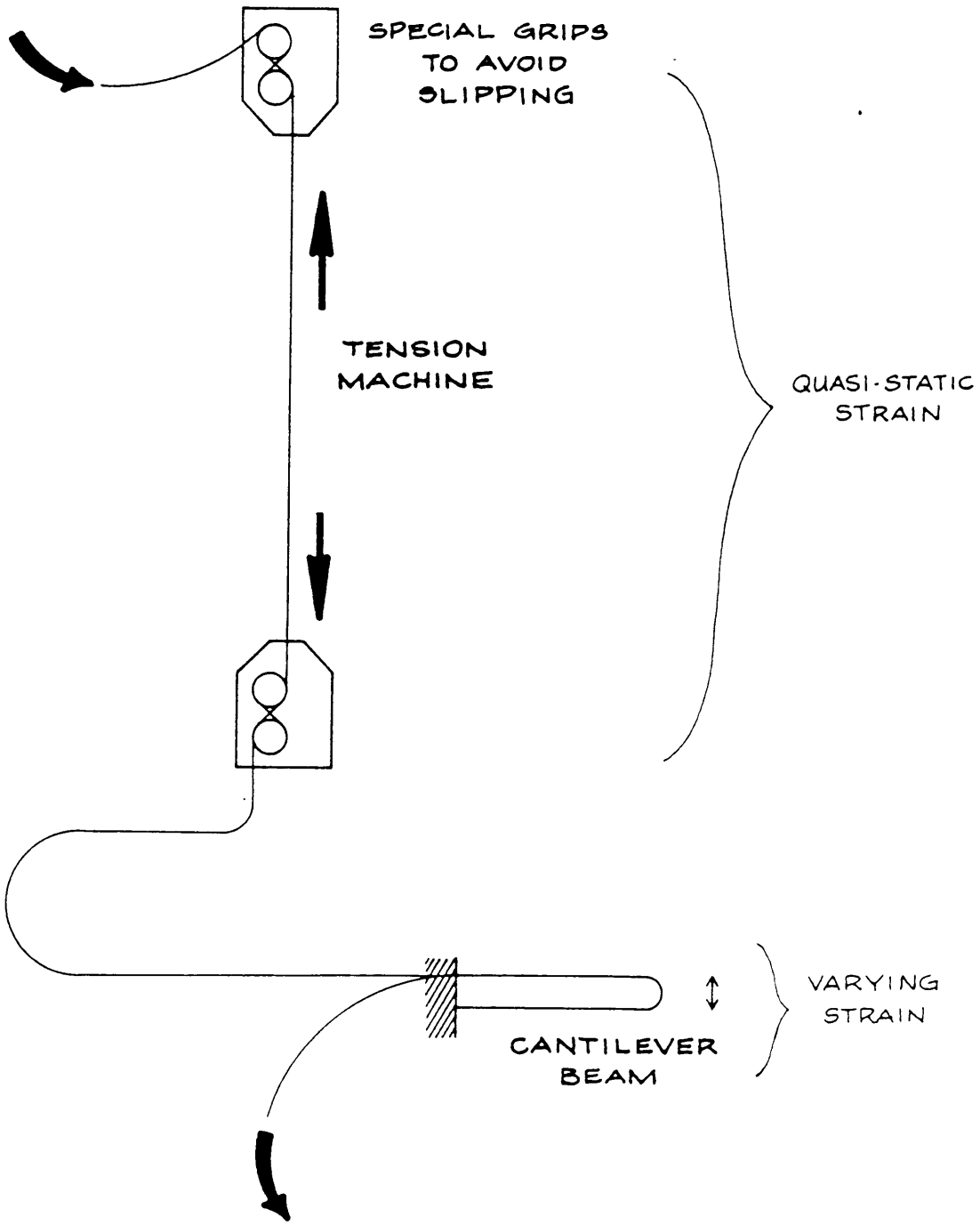

Figure 12. Strain application mechanism: The fiber was mounted with special grips on a tensile testing machine. Rates of displacement available are 0.1 to 50 mm/min. Another part of the fiber was bonded as a loop on a steel cantilever beam to enable vibrational strain at the fundamental frequency of 16 Hz.

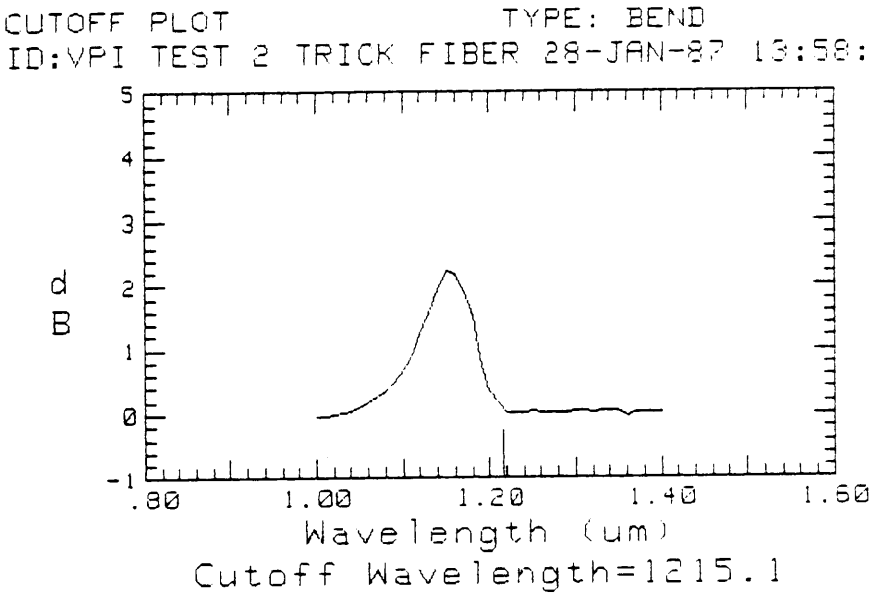

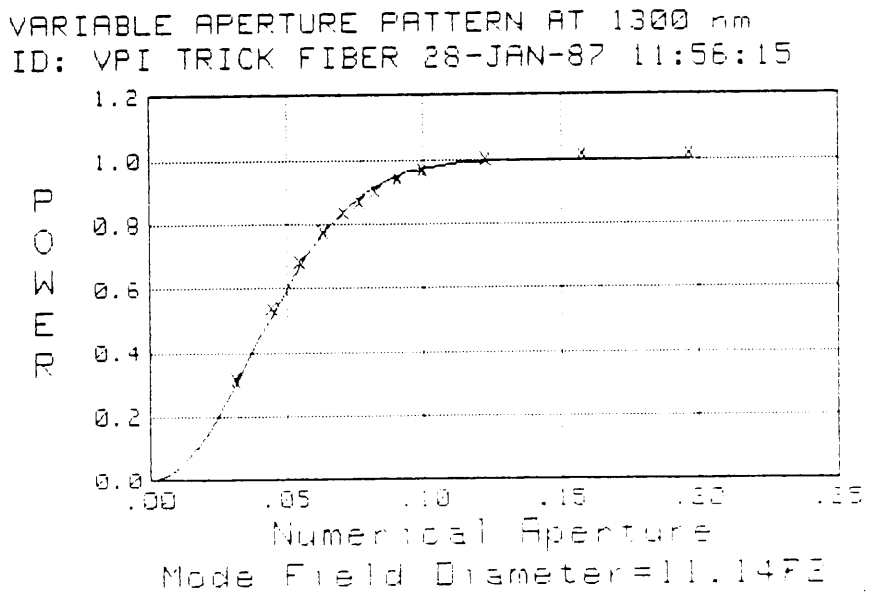

Figure 13. Optical fiber characterization: Tests conducted on Photon Kinetics FOA-2000 Fiber Analyzer.

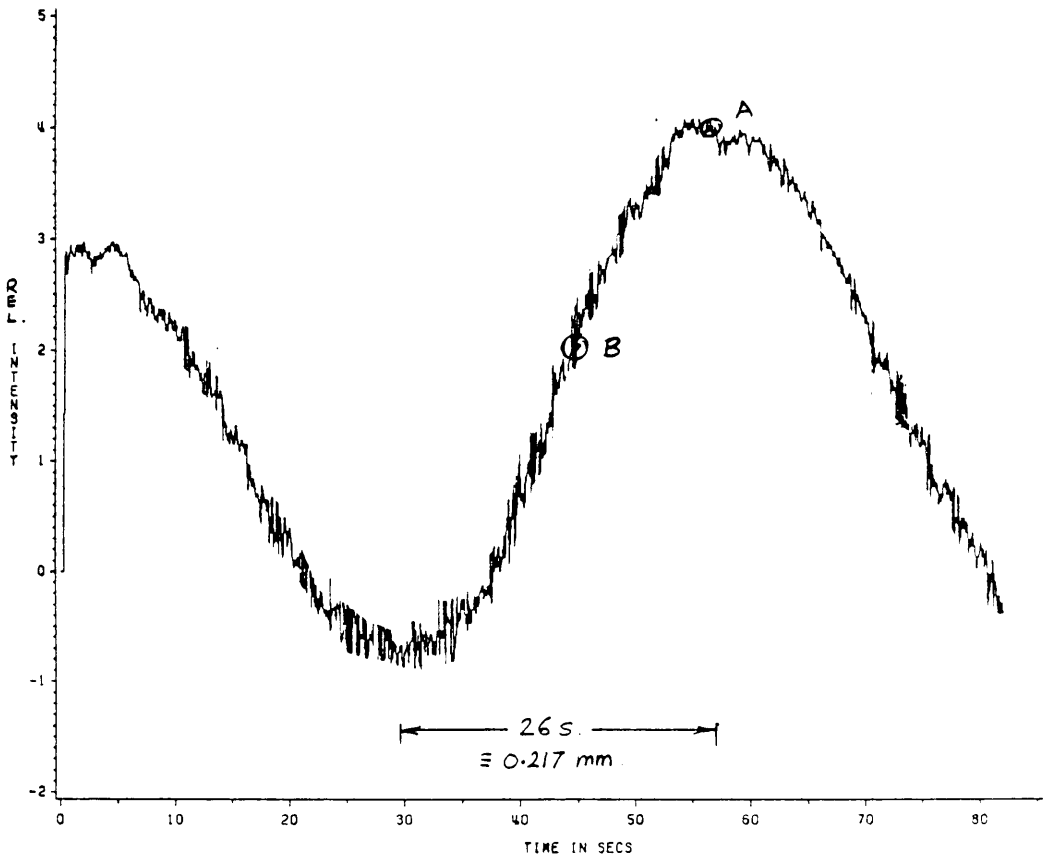

Figure 14. Axially strained optical fiber output-1: A displacement rate of 0.5 mm min has been applied axially on an optical fiber. This is the intensity variation at a fixed point on the pattern.

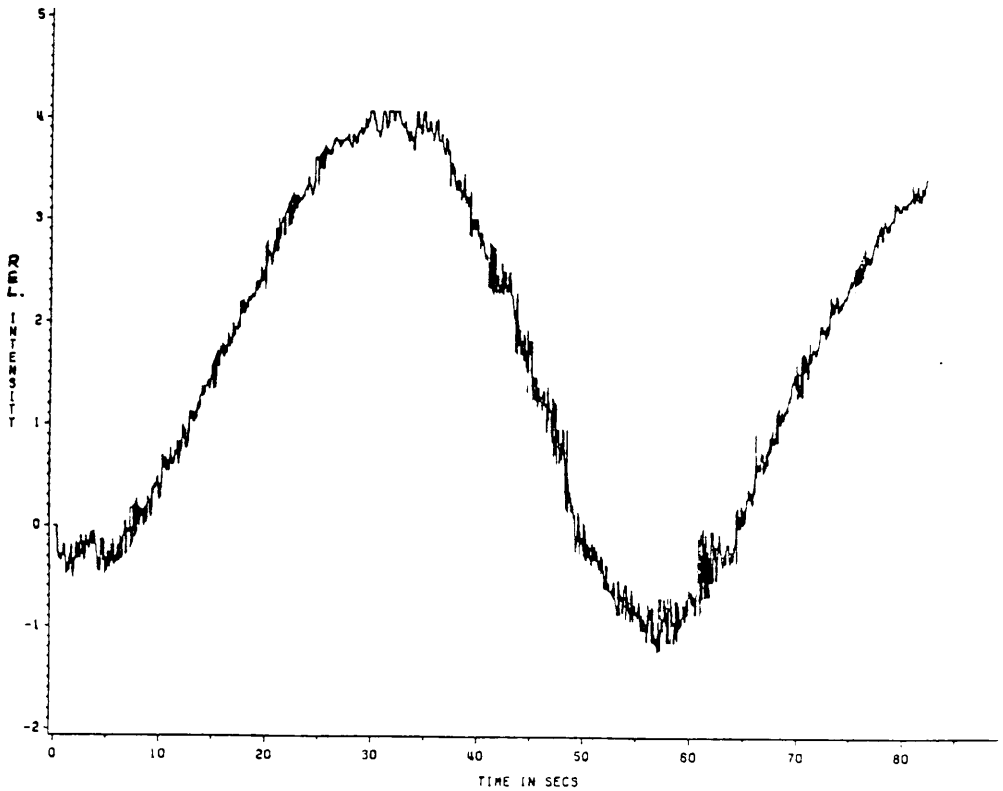

Figure 15. **Axially strained optical fiber output-2:** The strain applied in the previous figure is released at 0.5 mm min. This is the intensity variation at a fixed point on the pattern. This signal retraces the one obtained during tension.

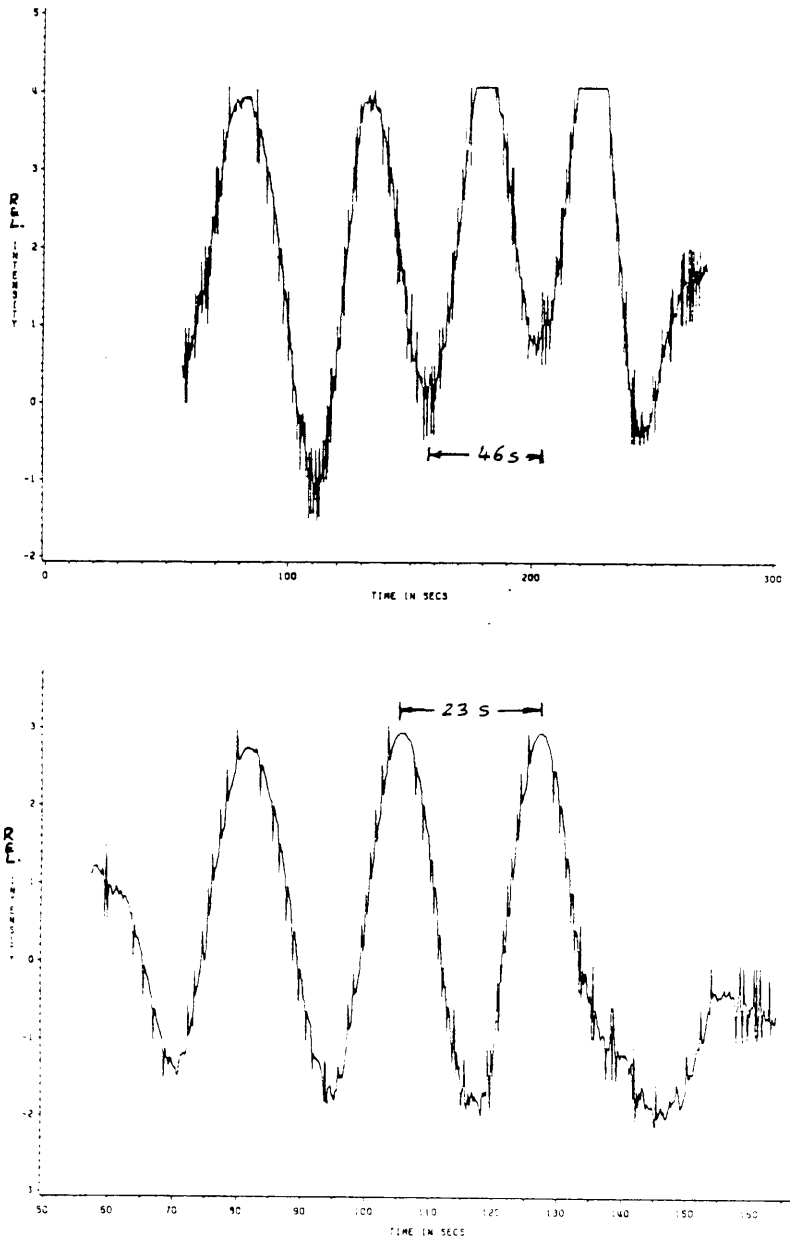

Figure 16. Axially strained optical fiber output-3: Displacement rates of 0.5 mm min and 1.0 mm min are applied axially on an optical fiber. Note the corresponding intensity variaiton rates.

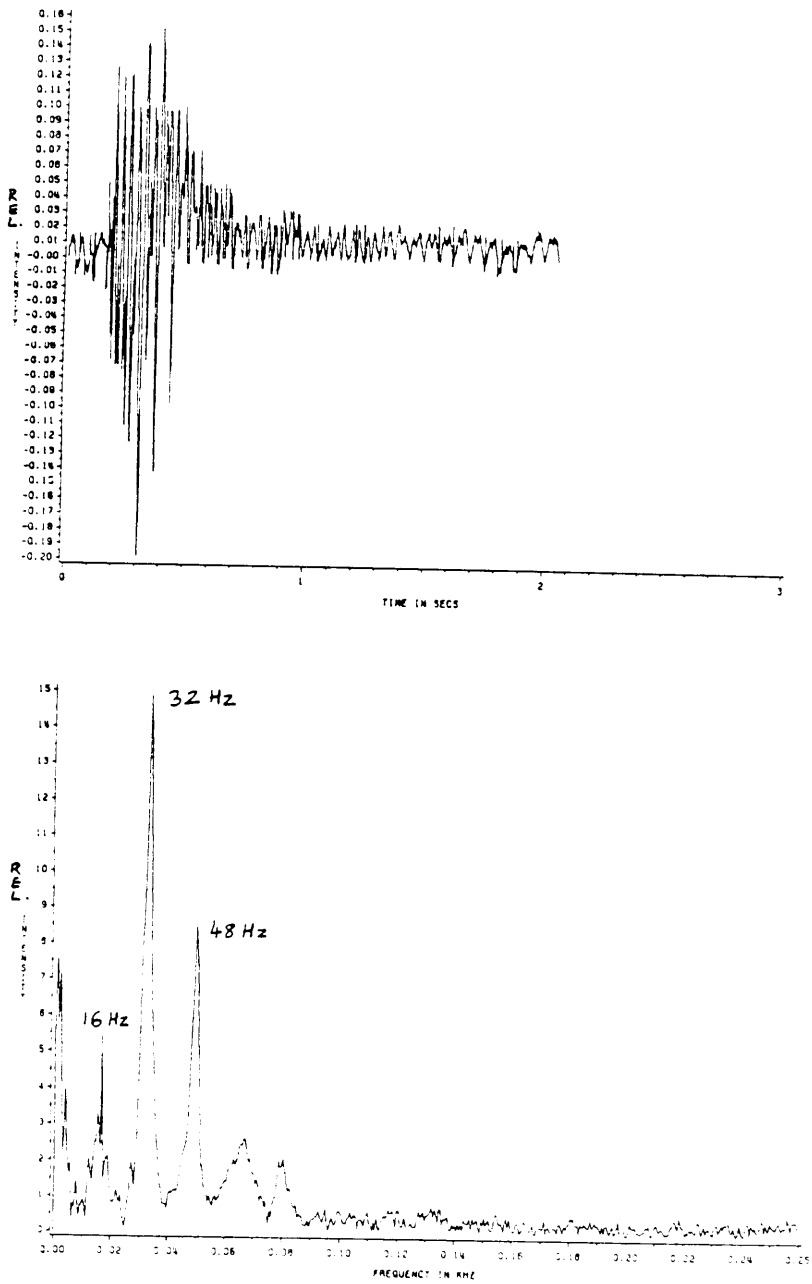

Figure 17. Vibrational strain in optical fibers-1.: Varying strain due to vibration are shown here as intensity changes. The quiescent point was A in Figure 14 on page 65. The bottom plot is the Fourier transform. Fundamental is at 16 Hz. The multiple components are due to non-linearity.

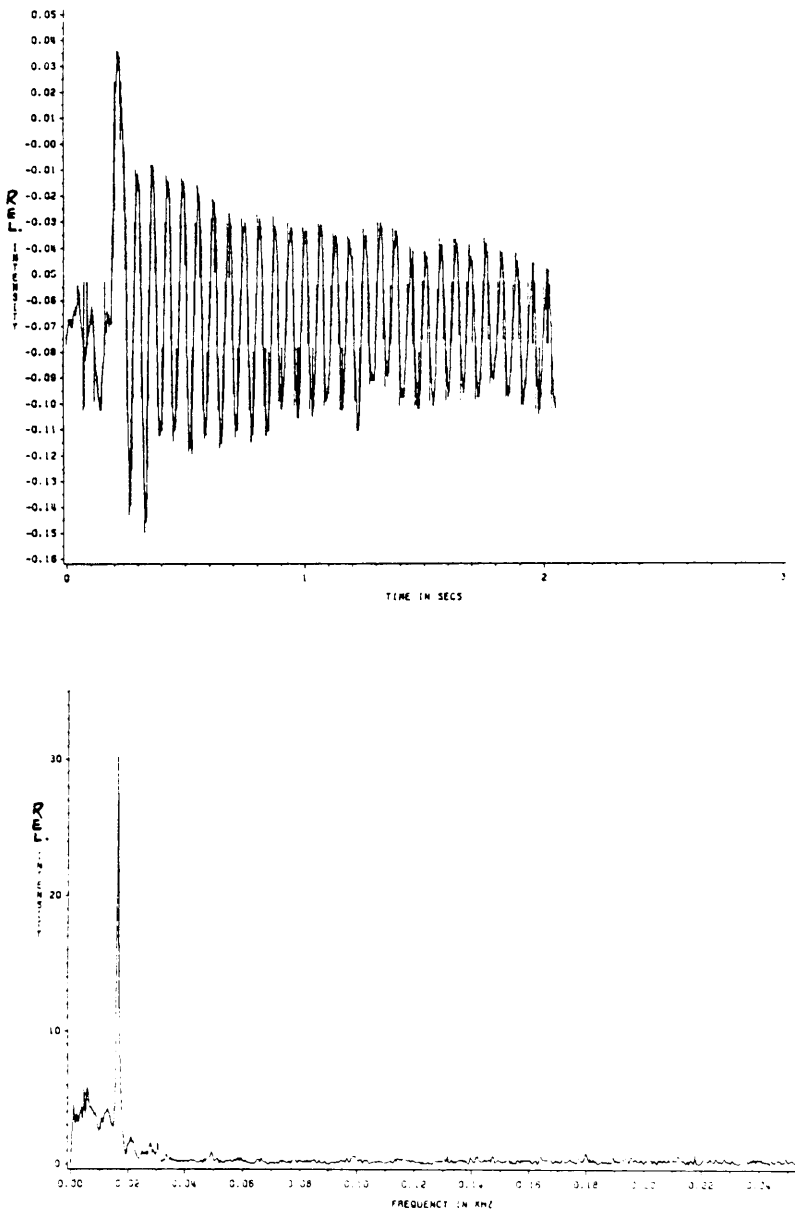

Figure 18. Vibrational strain in optical fibers-2.: Varying strain due to vibration are shown here as intensity changes. The quiescent point was B in Figure 14 on page 65. The bottom Fourier transform reveals the linear behaviour. The fundamental is at 16 Hz.

8.0 References

1. R.F. Harrington, "Time-harmonic electromagnetic fields," McGraw Hill, 1961

2. N.S.Kapany and J.J Burke, "Optical waveguides," Academic Press, 1972.

3. A.H. Cherin, "Introduction to optical fibers," McGraw-Hill, 1983

4. E.Snitzer, "Cylindrical dielectric waveguide modes," Journal of the Optical Society of America, vol 51, no 5, p491, May 1961

5. D.Gloge, "Weakly guiding fibers," Applied Optics, vol 10, no 7, p2252, Oct 1971

6. A.W.Snyder and J.D. Love, "Optical waveguide theory," Chapman and Hall, 1983

7. E.Snitzer and H.Osterberg, "Observed dielectric waveguide modes in the visible spectrum," Journal of the Optical Society of America, vol 51, no 5, p499, May 1961

8. C.D.Butter and G.B.Hocker, "Fiber optics strain gauge," Applied Optics, vol 17, no 18, p2867, Sept. 1978

9. W.Eickhoff, "Temperature sensing by mode-mode interference in birefringent optical fibers," Optics Letters, vol 6, no 4, p204, April 1981

10. J.A.Bucaro and E.F.Carome, "Single fiber interferometric acoustic sensor," Applied Optics, vol 17, no 3, p330, Feb. 1978

11. S.A.Kingsley and D.E.N.Davies, "Multimode optical fibre phase modulation and discrimination I & II," Electronics Letters, vol 14, no 11, p322/335, May 1978

12. M.R.Layton and J.A.Bucaro, "Optical fiber acoustic sensor utilizing mode-mode interference," Applied Optics, vol 18, no 5, p666, March 1979

13. P.A.Ehrenfeuchter, "Modal domain detection of vibration in beams," M.S.Thesis, Virginia Tech, Dec 1986.

14. N.K.Shankaranarayanan, K.D.Bennett, and R.O.Claus, "Optical fiber modal domain detection of stress waves," IEEE Ultrasonics Symposium, Williamsburg, VA, Nov 1986

The vita has been removed from the scanned document